ISSN 1560-3547, Regular and Chaotic Dynamics, 2019, Vol. 24, No. 3, pp. 329–352. © Pleiades Publishing, Ltd., 2019.

A Parabolic Chaplygin Pendulum and a Paul Trap: Nonintegrability, Stability, and Boundedness

Alexey V. Borisov[1,2*], **Alexander A. Kilin**[3**], **and Ivan S. Mamaev**[4,5***]

[1] *A. A. Blagonravov Mechanical Engineering Research Institute of RAS, ul. Bardina 4, Moscow, 117334 Russia*

[2] *Institute of Mathematics and Mechanics of the Ural Branch of RAS, ul. S. Kovalevskoi 16, Ekaterinburg, 620990 Russia*

[3] *Udmurt State University, ul. Universitetskaya 1, Izhevsk, 426034 Russia*

[4] *Moscow Institute of Physics and Technology, Institutskii per. 9, Dolgoprudnyi, 141700 Russia*

[5] *Center for Technologies in Robotics and Mechatronics Components, Innopolis University, ul. Universitetskaya 1, Innopolis, 420500 Russia*

Received March 28, 2019; revised April 26, 2019; accepted May 06, 2019

Abstract—This paper is a small review devoted to the dynamics of a point on a paraboloid. Specifically, it is concerned with the motion both under the action of a gravitational field and without it. It is assumed that the paraboloid can rotate about a vertical axis with constant angular velocity. The paper includes both well-known results and a number of new results. We consider the two most widespread friction (resistance) models: dry (Coulomb) friction and viscous friction. It is shown that the addition of external damping (air drag) can lead to stability of equilibrium at the saddle point and hence to preservation of the region of bounded motion in a neighborhood of the saddle point. Analysis of three-dimensional Poincaré sections shows that limit cycles can arise in this case in the neighborhood of the saddle point.

MSC2010 numbers: 37J25, 37J05

DOI: 10.1134/S1560354719030067

Keywords: parabolic pendulum, Paul trap, rotating paraboloid, internal damping, external damping, friction, resistance, linear stability, Hill's region, bifurcational diagram, Poincaré section, bounded trajectory, chaos, integrability, nonintegrability, separatrix splitting

INTRODUCTION

1. This paper gives a small review devoted to the dynamics of a material point on a paraboloid

$$x_3 = \frac{1}{2}\left(\frac{x_1^2}{a_1} + \frac{x_2^2}{a_2}\right).$$

It presents an analysis of motion both under the action of a gravitational field and without it. It is assumed that the paraboloid can rotate about the axis Ox_3 with constant angular velocity Ω. The paper includes well-known and a number of new results.

The main motivation for this work was the problem of a mechanical Paul trap [47] [1)], a hyperbolic paraboloid (saddle) which rotates about a vertical axis and on which a heavy ball rolls. Experiments show that, under a suitable choice of the angular velocity of rotation of the saddle Ω, the dimension and mass of the ball, the trajectory of the ball can remain in a neighborhood of the saddle point for a fairly long time [25](see also videos on [60, 61]). An open problem is to construct a sufficiently accurate model of this system that would take into account the effects of friction and allow an

*E-mail: borisov@rcd.ru
**E-mail: aka@rcd.ru
***E-mail: mamaev@rcd.ru

1) Wolfgang Paul was a German physicist who won a Nobel Prize in 1989.

analysis of the onset and change of various motion regimes depending on the system parameters. In particular, it would be very interesting to find an answer to the question of *whether there exist system parameters* (*and suitable initial conditions*) *under which the ball can remain in a neighborhood of the saddle point for an arbitrarily long time or such a boundedness is temporary.* At this point, we recall that, for example, the gyroscopic stabilization of a shell (bullet) is always temporary since it is destroyed by an arbitrarily small air drag [23].

If the analysis of this system is carried out by using the most general mechanical equations of motion with friction and resistance forces taken into account, then the corresponding system of equations is too complicated to make a complete analysis of its dynamics for all possible parameter values. Therefore, at the first stage it is necessary to use various simplifications of that dynamics. There are two natural approaches to the simplifications.

1) Investigation of the dynamics of a material point on a paraboloid. In this case, one ignores the inertial properties of the ball with respect to rotation, but it is possible to take into account various resistance forces [16, 19].
2) Analysis of the nonholonomic model of a ball rolling in a paraboloid [8, 9, 25]. This is the limit of the so-called absolutely rough surface. The dynamics of the system is conservative and does not allow an analysis of the effects caused by resistance.

The second approach, which involves investigation of nonholonomic systems and their application to describe the rolling of bodies on different surfaces, has been actively developed in recent years [3, 4, 11, 13, 15, 26, 35]. On the one hand, this avenue has yielded a qualitative description of some dynamical effects such as the reversal of a rattleback [12], the existence of chaotic regimes [7], etc. [53]. On the other hand, this avenue has made it possible to find effects [2, 17, 34, 50] which show that the applicability of nonholonomic models is limited, which is due to the fact that the work of friction and resistance forces is neglected.

In this paper, we focus on the first approach. The papers [16, 18, 19, 21, 46] show that the interest in the dynamics of a particle on a paraboloid (both elliptic and hyperbolic) arose long before the publication of the papers of Paul [47, 48] devoted to ion traps. For this reason, we have included the analysis of dynamics not only on a hyperbolic, but also on an elliptic paraboloid (in this case, the system is sometimes called a parabolic pendulum [21]). In addition, investigations of motion in an elliptic paraboloid may be simpler when it comes to verifying the model of the system by experiments.

A problem close to the problem of a parabolic pendulum was considered already by Huygens when he searched for isochronic circular oscillations important for designing clocks. In his work [31] he showed that, if one suspends a weight on a thread so that its end moves on the surface of the paraboloid of revolution, the period of the pendulum's rotation (i. e., precession) will not depend on the angle of its inclination. To realize this mechanism, Huygens suggested fastening the point of suspension of the thread at the top of an axisymmetric surface which is obtained by rotating some part of the semicubical parabola

$$y^2 = ax^3 + b$$

about the vertical (by analogy with a cycloidal pendulum).

Brower [18] considered the problem of a material point in an elliptic rotating paraboloid under the action of a gravitational field and dry (Coulomb) friction forces. He showed that the motion of a particle relative to the surface ceases in finite time and that the stop does not necessarily occur at the minimum point. Bottema [16] considered, instead of dry friction, the case of damping (viscous resistance) forces and proposed two models: internal damping and external damping. He analyzed the linear stability of equilibrium.

The other results obtained for this system also concern, as a rule, the analysis of the stability of equilibrium and numerical integration of individual trajectories [36, 38, 55, 57]. The results of this work clearly demonstrate that a detailed study of the dynamics of a point on a paraboloid for $\Omega \neq 0$ both in the absence and in the presence of friction cannot be accomplished by purely analytical methods. For example, the search for physically realizable bounded trajectories in a neighborhood of a saddle point can be carried out only by using a numerical analysis of the Poincaré section of the system. In the presence of friction the Poincaré map of the system turns out to be three-dimensional. Examples of investigation of some model and physical 3D Maps can be found in [20, 22, 24, 43, 44].

2. In Section 1 we discuss the problem of constructing integrable potentials for the dynamics of a particle on a stationary paraboloid. The paraboloid is considered as a limiting case of the general quadric, for which this problem (in the case of separation of variables) was solved in [5, 58]. Here we construct analogous polynomial and fractionally rational potentials for which the system is integrable. For this, we use a generating function which considerably simplifies the construction of these potentials. For the simplest potentials, we find explicitly an additional integral that generalizes the Joachimsthal integral for geodesics on an ellipsoid and the integral found in [29].

In Section 2 we derive equations of motion of a particle both with and without friction (resistance) forces. We consider the two most widespread models of friction (resistance):

– dry (Coulomb) friction, for which the friction force is proportional to the force of normal reaction;
– viscous friction, in which case friction is proportional to the velocity of the particle.

In the case of viscous friction we consider, following [16], two cases: internal damping, when the force is proportional to the velocity of the particle relative to the rotating surface, and external damping, when the force is proportional to the velocity of the particle relative to the fixed axes (from a physical point of view, it describes the air drag).

Section 3 gives a detailed treatment of the problem of frictionless motion of a material point on the surface of both a stationary and a rotating paraboloid. In the case of a stationary paraboloid, the system turns out to be integrable. For this system, we plot a bifurcation diagram that describes rearrangements of integral submanifolds and corresponding motion regimes. For the case of an elliptic paraboloid, we find critical periodic solutions and carry out an analysis of their stability. Using numerical analysis, we show that, in this case, asymptotic surfaces (separatrices) to unstable periodic solutions split when rotation is added ($\Omega \neq 0$), which shows nonintegrability of the system in the general case.

For a rotating paraboloid, we present results of the linear stability of equilibrium of a particle at the origin of coordinates, analyze rearrangements of Hill's regions [1] depending on the value of the energy integral and the system parameters. These analytical results do not provide a complete picture of the dynamics of the system. In particular, it is shown using numerical analysis of the Poincaré section that even in the case of unbounded Hill's regions the phase space can contain regions of bounded motion. Regions of existence of bounded motions on the plane of the energy integral and the angular velocity of rotation Ω are numerically plotted for some fixed ratios of the principal radii of curvature.

Section 4 treats the problem of the motion of a material point on the surface of a rotating paraboloid in the presence of viscous friction (damping) forces. A linear stability analysis for the case of a linear combination of internal and external damping forces is made. It is shown that, in the case of internal damping forces acting from the surface, the equilibrium at the vertex of the hyperbolic paraboloid is always unstable. However, the instability pattern allows one to interpret the behavior of the trajectories near equilibrium as temporary stability. It is also shown that the addition of external damping (air drag) can lead to stability of equilibrium at the saddle point and hence to preservation of the region of bounded motion in a neighborhood of the saddle point. The analysis of three-dimensional Poincaré sections shows that, in this case, asymptotically stable periodic solutions (limit cycles) may arise in the neighborhood of the saddle point.

For the sake of completeness we have added an appendix that includes the main results relating to the stability and conservativeness of linear systems of Newtonian type. We also note that in concrete examples it is usually not so much important to obtain inequalities expressing the stability conditions (which are sometimes too cumbersome), as it is to clearly represent these results either graphically or in the form of a physical (mechanical) description of the requirements concerning the system parameters.

1. INTEGRABLE POTENTIALS FOR A PARTICLE ON A STATIONARY PARABOLOID

The integrable Jacobi problem of geodesics on an ellipsoid [32] is well known. Its natural generalization is the problem of the motion of a particle on quadrics

$$\frac{x_1^2}{a_1} + \frac{x_2^2}{a_2} + \frac{x_3^2}{a_3} = 1 \tag{1.1}$$

in a given potential field $U(\boldsymbol{x})$, $\boldsymbol{x} = (x_1, x_2, x_3)$.

Potentials that are integrable by the method of separation of variables and are polynomial and rational (in the initial Cartesian coordinates) were found in [5, 58], see also [10].

A less known fact [10] is that these potentials can be obtained by a simpler method using the generating function

$$\Phi_z(\boldsymbol{x}) = \left(1 - \frac{x_1^2}{a_1 - z} - \frac{x_2^2}{a_2 - z} - \frac{x_3^2}{a_3 - z}\right)^{-1}. \tag{1.2}$$

When expanding $\Phi_z(\boldsymbol{x})$ in a power series of $1/z$ we obtain the polynomial potentials described above. Accordingly, the Taylor series expansion (1.2) in a neighborhood of some point $z = a_0 \neq 0$ gives the simplest rational integrable potentials.

We consider here the limiting case of the quadric (1.1), namely, the motion of a material point on a hyperbolic or an elliptic paraboloid

$$x_3 = \frac{1}{2}\left(\frac{x_1^2}{a_1} + \frac{x_2^2}{a_2}\right). \tag{1.3}$$

When $a_1a_2 < 0$, the paraboloid is hyperbolic, and when $a_1a_2 > 0$, it is elliptic.

To obtain the quadric (1.3), we need to make the substitution

$$x_1 \to x_1,\ x_2 \to x_2,\ x_3 \to x_3 - x_0,$$
$$a_1 \to a_1x_0, \quad a_2 \to a_2x_0, \quad a_3 \to x_0^2$$

in (1.1), multiply (1.1) by x_0 and perform the passage to the limit $x_0 \to \infty$. A similar passage to the limit in (1.2) with the additional transformation $z \to zx_0$ will give us a generating function of integrable potentials on the paraboloid

$$\Phi_z^{(p)}(\boldsymbol{x}) = \left(z - 2x_3 + \frac{x_1^2}{a_1 - z} + \frac{x_2^2}{a_2 - z}\right)^{-1}. \tag{1.4}$$

The coefficients in the expansion of this function in powers of z^{-1} give polynomial integrable potentials:

$$U_2 = 2x_3, \quad U_3 = 4x_3^2 + x_1^2 + x_2^2, \quad U_4 = 8x_3^3 + 4x_3(x_1^2 + x_2^2) + a_1x_1^2 + a_2x_2^2, \quad \ldots.$$

In a similar way, from the expansion in a neighborhood of $z = a_0 \neq 0$ we find rational potentials of the form

$$V_0 = \Phi_z^{(p)}(a_0) = \left(a_0 - 2x_3 + \frac{x_1^2}{a_1 - a_0} - \frac{x_2^2}{a_2 - a_0}\right)^{-1},\ V_1 = V_0^2\left(1 + \frac{x_1^2}{(a_1 - a_0)^2} + \frac{x_2^2}{(a_2 - a_0)^2}\right), \ldots.$$

To prove this fact, we define the parabolic coordinates (u, v) as the roots of the equation

$$z - 2x_3 + \frac{x_1^2}{a_1 - z} + \frac{x_2^2}{a_2 - z} = 0.$$

This yields

$$x_1^2 = \frac{a_1(a_1 - u)(a_2 - v)}{a_2 - a_1}, \quad x_2^2 = \frac{a_2(a_2 - u)(a_2 - v)}{a_1 - a_2}, \quad x_3 = \frac{1}{2}(u + v - a_1 - a_2).$$

The kinetic energy of a material point of unit mass on a paraboloid is written as

$$T = \frac{1}{2}(\dot{x}_1^2 + \dot{x}_2^2 + \dot{x}_3^2) = \frac{u - v}{4}\left(\frac{u\dot{u}^2}{(a_1 - u)(a_2 - u)} - \frac{v\dot{v}^2}{(a_1 - v)(a_2 - v)}\right),$$

and the potential (1.4) is written as

$$\Phi_z^{(p)} = (u - v)^{-1}\left(\frac{a_1a_2}{z}\left(\frac{1}{v} - \frac{1}{u}\right) + \frac{a_1a_2 - (a_1 + a_2)u + u^2}{u(z - u)} - \frac{a_1a_2 - (a_1 + a_2)v + v^2}{v(z - v)}\right).$$

Thus, the variables are separated at any value of z, and hence every term in the expansion in this parameter defines the separable potential.

An additional integral can also be found by the method of separation of variables. We present it explicitly for the case of the potential

$$U = \mu x_3 + \frac{c_1}{x_1^2} + \frac{c_2}{x_2^2}.$$

This integral, which generalizes the well-known Joachimsthal integral in the problem of geodesics on an ellipsoid, has the form

$$F = \left(1 + \frac{x_1^2}{a_1^2} + \frac{x_2^2}{a_2^2}\right)\left(\frac{\dot{x}_1^2}{a_1} + \frac{\dot{x}_2^2}{a_2} + \mu + \frac{2c_1}{a_1}\frac{1}{x_1^2} + \frac{2c_2}{a_2}\frac{1}{x_2^2}\right).$$

For $c_1 = c_2 = 0$, an integral in explicit form was found in [29].

2. A PARTICLE IN A GRAVITATIONAL FIELD ON A ROTATING PARABOLOID

2.1. Equations of Motion, Various Friction Models

We now consider the problems of stability and destabilization of motion of a material point in a gravitational field on a rotating paraboloid (1.3). Making the scaling transformation $x_k \to a_1 x_k$, $k = 1, 2, 3$, we represent the surface equation as

$$x_3 = \frac{1}{2}\big(x_1^2 + bx_2^2\big), \quad b = \frac{a_1}{a_2}. \tag{2.1}$$

When $b > 0$, the paraboloid is elliptic, and when $b < 0$, it is hyperbolic.

In a (noninertial) coordinate system $Ox_1x_2x_3$, which rotates together with the surface (2.1), for a point of unit mass the Lagrangian of the system can be represented as

$$L = \frac{1}{2}\Big((\dot{x}_1 - \Omega x_2)^2 + (\dot{x}_2 + \Omega x_1)^2 + (x_1\dot{x}_1 + bx_2\dot{x}_2)^2\Big) - \frac{1}{2}g\big(x_1^2 + bx_2^2\big), \tag{2.2}$$

where Ω is the angular velocity of rotation of the paraboloid and g is the free-fall acceleration.

The corresponding equations of motion are

$$\begin{gathered}\left(\frac{\partial L}{\partial \dot{\boldsymbol{x}}}\right)^{\displaystyle\cdot} - \frac{\partial L}{\partial \boldsymbol{x}} = \boldsymbol{Q},\\ \boldsymbol{x} = (x_1, x_2), \quad \boldsymbol{Q} = \left(Q_1^{(0)} + Q_3^{(0)}\frac{\partial x_3}{\partial x_1},\, Q_2^{(0)} + Q_3^{(0)}\frac{\partial x_3}{\partial x_2}\right),\end{gathered} \tag{2.3}$$

where $\big(Q_1^{(0)}, Q_2^{(0)}, Q_3^{(0)}\big)$ is the three-dimensional vector of nonpotential forces acting on the material point in $\mathbb{R}^3$; this vector is assumed to be tangent to the surface (2.1).

If $\boldsymbol{Q} = 0$, then the system admits the energy integral

$$E = \frac{1}{2}\big(\dot{x}_1^2 + \dot{x}_2^2 + (x_1\dot{x}_1 + bx_2\dot{x}_2)^2\big) - \frac{\Omega^2}{2}(x_1^2 + x_2^2) + \frac{g}{2}\big(x_1^2 + bx_2^2\big). \tag{2.4}$$

As we see, for integrability we need another additional integral. Below (see Section 3) it will be shown using numerical simulation that in the general case, when $\Omega \neq 0$, there exists no additional integral.

Remark. The equations of motion (2.3) are obtained from the Lagrange equations in redundant variables (x_1, x_2, x_3) [1] with an undetermined multiplier, by eliminating this multiplier and the redundant coordinate x_3.

It should be kept in mind that it is the three-dimensional vector of external forces $\boldsymbol{Q}^{(0)}$ that is found from physical or mechanical considerations (experiments). On the other hand, it is less convenient to analyze the dynamics of this system in redundant variables. This is why we have passed to equations (2.3).

Possible friction forces dealt with in [16, 18] are as follows.

1°. *Internal viscous friction* (internal damping), for which the drag force opposes the relative velocity of the point:

$$Q_1^{(0)} = -\mu\dot{x}_1, \quad Q_2^{(0)} = -\mu\dot{x}_2, \quad Q_3^{(0)} = -\mu\dot{x}_3,$$

where μ is the coefficient of friction. Substituting into (2.3) gives

$$\boldsymbol{Q} = -\hat{\boldsymbol{\mu}}\dot{\boldsymbol{x}} = -\frac{\partial R^i}{\partial \dot{\boldsymbol{x}}},$$
$$R^i = \frac{1}{2}(\dot{\boldsymbol{x}}, \hat{\boldsymbol{\mu}}\dot{\boldsymbol{x}}), \quad \hat{\boldsymbol{\mu}} = \mu \begin{pmatrix} 1 + x_1^2 & bx_1x_2 \\ bx_1x_2 & 1 + b^2x_2^2 \end{pmatrix}, \tag{2.5}$$

where R^i is the Rayleigh function and $\hat{\boldsymbol{\mu}}$ is a positive definite matrix.

2°. *External viscous friction* (for example, air drag). In this case, the friction force opposes the velocity of the point in the fixed coordinate system:

$$Q_1^{(0)} = -\mu(\dot{x}_1 - \Omega x_2), \quad Q_2^{(0)} = -\mu(\dot{x}_2 + \Omega x_1), \quad Q_3^{(0)} = -\mu\dot{x}_3.$$

In this case, we find

$$\boldsymbol{Q} = -\hat{\boldsymbol{\mu}}\dot{\boldsymbol{x}} + \hat{\mathbf{D}}\boldsymbol{x}, \quad \hat{\mathbf{D}} = \begin{pmatrix} 0 & \mu\Omega \\ -\mu\Omega & 0 \end{pmatrix},$$

where $\hat{\boldsymbol{\mu}}$ is a 2×2 matrix defined in (2.5).

3°. *Dry friction:*

$$Q_1^{(0)} = -\frac{\mu N}{v}\dot{x}_1, \quad Q_2^{(0)} = -\frac{\mu N}{v}\dot{x}_2, \quad Q_3^{(0)} = -\frac{\mu N}{v}\dot{x}_3,$$
$$v = \sqrt{\dot{x}_1^2 + \dot{x}_2^2 + \dot{x}_3^2},$$
$$N = \frac{g + \dot{x}_1^2 + b\dot{x}_2^2 + 2\Omega(x_1\dot{x}_2 - bx_2\dot{x}_1) + \Omega^2(x_1^2 + bx_2^2)}{\sqrt{1 + x_1^2 + b^2x_2^2}},$$

where N is the value of the reaction force. Thus, we obtain

$$\boldsymbol{Q} = -\frac{N}{v}\hat{\boldsymbol{\mu}}\dot{\boldsymbol{x}}, \tag{2.6}$$

where $\hat{\boldsymbol{\mu}}$ is also the matrix from (2.5).

2.2. The Problem of Stability of the Equilibrium Point

It follows from (2.3) that, in the case 1°, 2° and in the case without friction, the origin of coordinates

$$x_1 = x_2 = 0, \quad \dot{x}_1 = \dot{x}_2 = 0$$

is an equilibrium point. Its stability is the focus of our study.

By suitably rescaling the axes the problem of *linear stability* can be reduced to analysis of a four-dimensional system of special type. Using the two-dimensional vectors $\boldsymbol{x} = (x_1, x_2)$, $\boldsymbol{v} = (v_1, v_2)$, we write it in vector form as

$$\begin{gathered} \dot{\boldsymbol{x}} = \boldsymbol{v}, \quad \dot{\boldsymbol{v}} = -\hat{\mathbf{C}}(\boldsymbol{\alpha})\boldsymbol{x} + \hat{\mathbf{D}}(\boldsymbol{\alpha})\boldsymbol{x} - \hat{\boldsymbol{\mu}}(\boldsymbol{\alpha})\boldsymbol{v} + \hat{\boldsymbol{\omega}}(\boldsymbol{\alpha})\boldsymbol{v}, \\ \hat{\mathbf{C}} = \hat{\mathbf{C}}^T, \quad \hat{\mathbf{D}} = -\hat{\mathbf{D}}^T, \quad \hat{\boldsymbol{\mu}} = \hat{\boldsymbol{\mu}}^T, \quad \hat{\boldsymbol{\omega}} = -\hat{\boldsymbol{\omega}}^T, \end{gathered} \tag{2.7}$$

where $\hat{\mathbf{C}}$, $\hat{\mathbf{D}}$, $\hat{\boldsymbol{\mu}}$, $\hat{\boldsymbol{\omega}}$ are 2×2 matrices depending on the parameters $\boldsymbol{\alpha} = (\alpha_1 \ldots \alpha_m)$ of the initial system.

In this case, $\boldsymbol{\alpha} = (g, b, \Omega)$ and, regardless of the law of friction, we have

$$\hat{\mathbf{C}} = \begin{pmatrix} g - \Omega^2 & 0 \\ 0 & gb - \Omega^2 \end{pmatrix}, \quad \hat{\boldsymbol{\omega}} = \begin{pmatrix} 0 & 2\Omega \\ -2\Omega & 0 \end{pmatrix}. \tag{2.8}$$

Hence, for case 1° we additionally obtain

$$\hat{\mathbf{D}} = 0, \quad \hat{\boldsymbol{\mu}} = \begin{pmatrix} \mu & 0 \\ 0 & \mu \end{pmatrix}. \tag{2.9}$$

For case 2°:

$$\hat{\mathbf{D}} = \begin{pmatrix} 0 & \mu\Omega \\ -\mu\Omega & 0 \end{pmatrix}, \quad \hat{\boldsymbol{\mu}} = \begin{pmatrix} \mu & 0 \\ 0 & \mu \end{pmatrix}. \tag{2.10}$$

Remark. In the case of dry friction (2.6), the problem of stability of the equilibrium point $x_1 = x_2 = 0$ loses its significance. As shown in [18], if a material point reaches a state of rest, it does so in finite time. Note that the end point of the trajectory may or may not coincide with the origin of the coordinate system, i. e., with the vertex (when $b > 0$) or with the saddle point (when $b < 0$) of the paraboloid.

3. FRICTIONLESS MOTION OF A PARTICLE

We first consider the motions of a particle in the absence of friction. To start with, we analyze the simplest integrable case with $\Omega = 0$.

3.1. An Integrable Case with $\Omega = 0$

As noted above (Section 1), in this case the system admits two quadratic integrals: the energy integral and generalizations of the Joachimsthal integral:

$$\begin{gathered} E = \frac{1}{2}\big(\dot{x}_1^2 + \dot{x}_2^2 + (x_1\dot{x}_1 + bx_2\dot{x}_2)^2\big) + \frac{g}{2}(x_1^2 + bx_2^2), \\ F = (1 + x_1^2 + b^2x_2^2)(\dot{x}_1^2 + b\dot{x}_2^2 + g). \end{gathered} \tag{3.1}$$

In this case, the separating variables are given by

$$x_1^2 = \frac{(u-1)(v-1)}{b^{-1}-1}, \quad x_2^2 = \frac{(b^{-1}-u)(v-b^{-1})}{b(b^{-1}-1)}.$$

Depending on the sign of b, the variables u and v are defined in the following intervals:

$$b > 0, \quad 0 < \min(1, b^{-1}) \leqslant u \leqslant \max(1, b^{-1}) \leqslant v;$$

$$b < 0, \quad u \leqslant b^{-1} < 0, \quad 1 \leqslant v.$$

The corresponding coordinate lines are shown in Fig. 1.

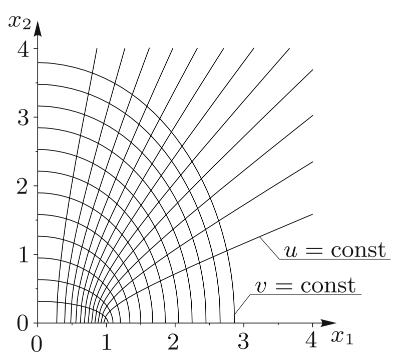

(a) $b = \frac{1}{2} > 0$

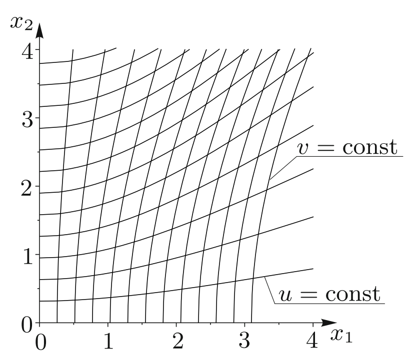

(b) $b = -\frac{1}{2} < 0$

Fig. 1. Coordinate grid of separating variables u and v on the plane x_1, x_2.

On the level surface of the first integrals (3.1), which is given by the relations $E = gh$ and $F = gk$, the evolution of the variables u and v is given by

$$\begin{gathered} \dot{u}^2 = \frac{4g}{(v-u)^2}\frac{(u-1)(b^{-1}-u)}{u}R_2(u), \quad \dot{v}^2 = -\frac{4g}{(v-u)^2}\frac{(v-1)(v-b^{-1})}{v}R_2(v), \\ R_2(z) = z^2 - (2h + 1 + b^{-1})z + kb^{-1}. \end{gathered} \tag{3.2}$$

Here and in what follows, when $b > 0$, we assume without loss of generality that $b < 1$.

We now find the values of the parameters k and h at which a rearrangement of the regions of possible motion occurs on the plane (x_1, x_2). According to (3.2), these values of k and h correspond to situations where one of the roots of the polynomial $R_2(z)$ is equal either to 1 or to b^{-1} or correspond to the case where the discriminant $R_2(z)$ vanishes. On the plane $\mathbb{R}^2 = \{(k, h)\}$, these values of the integrals form bifurcation curves, see Fig. 2:

$\gamma_1:\ k = 1 + 2h$, with $R_2(b^{-1}) = 0$;

$\gamma_2:\ k = 1 + 2bh$, with $R_2(1) = 0$;

$\gamma_3:\ 4bk = (1 + b + 2bh)^2$, with the discriminant $R_2(z)$ equal to zero.

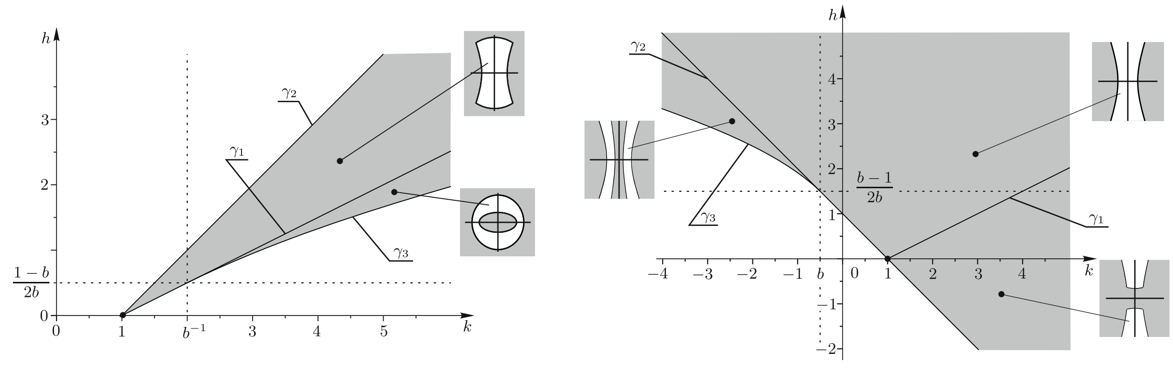

(a) $b > 0\,(b = 1/2)$ (b) $b < 0\,(b = -1/2)$

Fig. 2. Bifurcation diagram and projections of the regions of possible motion onto the plane (x_1, x_2). Grey denotes the region of possible values of k and h.

According to (3.2), when the values of the parameters k and h lie on the curves γ_1, γ_2 and γ_3, the initial system (2.3) possesses critical solutions which turn out to be periodic when $b > 0$. Thus, we see that, when $\Omega = 0$, the system (2.3) has the following families of critical solutions:

– two families (the curves γ_1, γ_2) of planar motions in the principal planes of the paraboloid;

– the curve γ_3 with $b > 0$ corresponds to two families of elliptic closed trajectories, which differ only in the direction of motion along them, and when $b < 0$, this curve corresponds to families of hyperbolic nonclosed trajectories.

In addition to these curves, we show in grey the regions of possible values of these quantities on the plane (k, h) (in other words, when k and h are chosen outside these regions, the equations $E = gh$ and $F = gk$ admit no real solutions for the variables x_k, $\dot{x}_k$, $k = 1, 2$). Thus, we obtain a bifurcation diagram of this integrable Hamiltonian system. Each point in the region of possible values $k, h \notin \gamma_k$, $k = 1, 2, 3$ corresponds in phase space to one or several invariant (Liouville) tori, and when the curves γ_k, $k = 1, 2, 3$, are intersected, rearrangements of these tori occur.

Thus, we see that, when $b > 0$, the curves γ_1 and γ_2 correspond to *periodic pendulum motions* in the principal planes of the paraboloid, and the curve γ_3 corresponds to *periodic motions in elliptic* (*in projection*) *orbits*. As is well known [6], if the bifurcation curves lie on the boundary of a bifurcation diagram (more precisely, a bifurcation complex), then the corresponding periodic solutions are stable. This leads us to the following conclusion:

1) *pendulum motions in the plane with the largest principal radius* (*the curve* γ_2) *are always stable;*

2) *elliptic periodic solutions* (*the curve* γ_3) *are always stable;*

3) *pendulum solutions in the plane with the smallest principal radius are stable for* $k < b^{-1}$ *and unstable* (*the curve* γ_1) *for* $k > b^{-1}$.

3.2. A Nonintegrable Case with $\Omega \neq 0$

We now turn to analysis of the general case of a particle moving on a rotating paraboloid. As will be shown below, by using a numerical construction of a Poincaré section, the system is found to be nonintegrable. Of particular interest in this case is the problem of the existence of particles' trajectories which remain, as $t \to \infty$, in a bounded region in a neighborhood of the origin of coordinates. We consider three approaches to this problem:

– analysis of linear stability;

– construction of Hill's regions;

– numerical investigation using a Poincaré section.

1. Linear stability of equilibrium points

We briefly describe the well-known results [16]), which pertain to the stability of the equilibrium point of the system (2.3) with $\Omega \neq 0$. As is well known [23], this stability with $b < 0$ is formal from a mathematical point of view since it is destroyed by adding an arbitrarily small friction (see the Appendix, Table 2). Nevertheless, from a physical point of view this stability is of great importance (for details, see [23]). Here and in what follows, we use the notation

$$\bar{\Omega} = \frac{\Omega}{\sqrt{g}}.$$

Case $b > 0$ — an elliptic paraboloid. According to (2.8) and Table 2 (lines 1 and 2) in the Appendix, the stability conditions in this case can be written as

– for small $|\Omega|$ the equilibrium point is linearly stable under the condition

$$\bar{\Omega}^2 < \min(1, b); \tag{3.3}$$

– for large $|\Omega|$ stability arises under the condition

$$\bar{\Omega}^2 > \max(1, b).$$

As is easy to verify, the second of the stability conditions is satisfied (see Table 1, line 2):

$$4\bar{\Omega}^2 > \left(\sqrt{\bar{\Omega}^2 - 1} + \sqrt{\bar{\Omega}^2 - b}\right)^2.$$

Case $b < 0$ — a hyperbolic paraboloid (saddle). Using in a similar way relations (2.8) and Table 2 in the Appendix, we find conditions for stability of the equilibrium point at the saddle point:

– *when* $\quad -1 < b, \quad 1 < \bar{\Omega}^2;$

– *when* $\quad b < -1, \quad 1 < \bar{\Omega}^2 < -\frac{(1-b)^2}{8(1+b)}.$

Summarizing the above, we represent the stability regions of the equilibrium point on the plane $(\bar{\Omega}^2, b)$, see also [16].

Thus, we see that at sufficiently large $\bar{\Omega}^2$ (in the case of an elliptic paraboloid, $b > 0$ and $\bar{\Omega}^2 > \max(1, b)$, and in the case of a saddle, $b < 0$ and $\bar{\Omega}^2 > 1$), the number of unstable degrees of freedom becomes even (it coincides with the number of negative eigenvalues of the matrix $\hat{\mathbf{C}}$ in (2.7)). Consequently, according to Thomson's theorem [23, 56] a gyroscopic stabilization (which explains the stability regions shown by hatching in Fig. 3) is possible.

To carry out a nonlinear stability analysis in the case (3.3), it suffices to use the method of Lyapunov functions. The role of a Lyapunov function is played by the energy integral (2.4). In the gyroscopic case, the proof of nonlinear stability requires using the KAM theorem and analyzing the condition for the absence of resonance and the twisting condition (for applications, see, e. g., [1, 46]).

Remark. If we omit centrifugal forces from consideration when calculating unstable degrees of freedom, as was done in [16], then this will lead to an incorrect conclusion that Thomson's theorem does not hold.

We formulate some conclusions.

1. *It is impossible to stabilize the equilibrium point on the saddle* ($b < 0$) *if* $\bar{\Omega}^2 < 1$ *or* $|b| > 3$ (*i. e., in the case of slow rotation and very steep saddles*).

2. *Both on an elliptic and on a hyperbolic paraboloid, the stability region is unbounded in* $\bar{\Omega}^2$.

3. *For every* (*noncircular*) *elliptic paraboloid* ($0 < b \neq 1$) *one can choose a rotational velocity* $\bar{\Omega}$ *at which the equilibrium point is unstable* (*gyroscopic destabilization*).

4. *For every elliptic paraboloid one can choose a rotational velocity* $\bar{\Omega}$ *at which the stability of the equilibrium point is disturbed.*

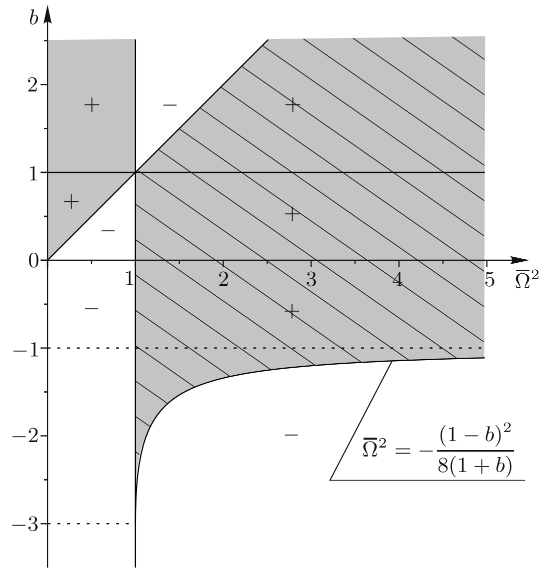

Fig. 3. Regions of stability (grey) and instability (white) of the equilibrium point on the parameter plane $(\bar{\Omega}^2, b)$. The region of gyroscopic stabilization is hatched.

2. Hill's regions

In addition to the stability analysis of equilibrium points, for some mechanical systems it is possible to establish that the trajectory remains in a bounded region of configuration space. Bounded regions of configuration space are defined from the condition of nonnegativeness of the kinetic energy on a given level set $E = \text{const}$ of the energy integral (2.4). These regions are analogs of Hill's regions in celestial mechanics [1]. For convenience, we will call them *Hill's regions* throughout the remainder of the text.

In this case, we fix the level set of the energy integral as follows:

$$E = gh, \quad h = \text{const}$$

and analyze the form of the regions of possible motion on the plane (x_1, x_2) depending on the values of the parameters $\bar{\Omega}^2$, b and the level set of the energy integral h.

Expressing the kinetic energy from (2.4) and using its positive definiteness, we obtain an inequality that defines possible values of the coordinates:

$$\frac{1}{g}T = h - \frac{1}{2}\big(1 - \bar{\Omega}^2\big)x_1^2 - \frac{1}{2}\big(b - \bar{\Omega}^2\big)x_2^2 \geqslant 0. \tag{3.4}$$

In other words, the region bounded by inequality (3.4) is a projection of the isoenergetic submanifold $\mathcal{M}_h^3$ onto configuration space, in this case onto the plane $\mathbb{R}^2 = \{(x_1, x_2)\}$.

We see that the boundary of Hill's region in this case is given by a second-order curve whose type and position are determined by the signs of the coefficients at x_1^2 and x_2^2 in (3.4). Thus, the parameter plane $(\bar{\Omega}^2, b)$ is partitioned by the straight lines

$$\bar{\Omega}^2 = 1 \quad \text{and} \quad \bar{\Omega}^2 = b \tag{3.5}$$

into four regions. In each of these regions, when the sign of h is changed, the rearrangements of Hill's regions are of the same type.

Figure 4 shows the parameter plane $(\bar{\Omega}^2, b)$ with the straight lines (3.5) shown on it. The regions corresponding to different types of Hill's regions are shown as hatched or crosshatched areas. Grey denotes the parameter region corresponding to bounded Hill's regions with $h \geqslant 0$. Hill's regions themselves (with $h \geqslant 0$ and $h < 0$) are also shown.

Thus, it is evident from Fig. 4 that Hill's regions are bounded only if the parameters lie in region a and are given by the inequality

$$b > 0, \quad \bar{\Omega}^2 < \min(1, b), \quad h \geqslant 0. \tag{3.6}$$

Therefore, the method of Hill's regions, too, provides no explanation for the existence of bounded trajectories in the Paul trap (i. e., when $b < 0$).

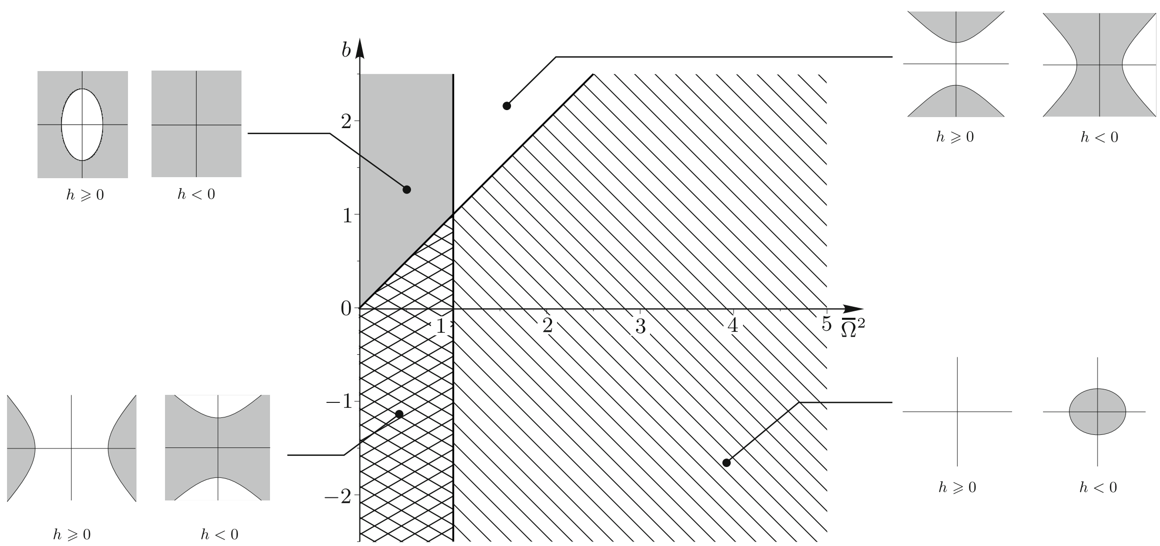

Fig. 4. Regions on the parameter plane $(\bar{\Omega}^2, b)$ which correspond to different types of Hill's regions. Hill's regions on the plane are shown in white (i. e., in the grey regions, motion is impossible).

3. A Poincaré map

We see that analytic investigations can in many cases give no answer to the question of existence of bounded trajectories near the vertex of a paraboloid. For this reason we will find out what can be established by numerical analysis.

To investigate the phase flow (2.7), (2.8) without friction ($\hat{D} = 0$, $\hat{\mu} = 0$), we use the method of constructing a Poincaré map. In this paper, the plane $x_1 = 0$ is chosen as a secant, and the Poincaré map is plotted in the variables (x_2, v_2).

As a rule, this method can be used only in the case where the recurrence of trajectories is observed. For this system, this occurs in the following cases:

– when the isoenergetic submanifold is bounded,

– near stable periodic solutions.

The first case takes place when inequalities (3.6) are satisfied. Indeed, the fact that Hill's region is bounded and the positive definiteness of the kinetic energy as a quadratic form in velocities imply that the isoenergetic submanifold is bounded in the entire phase space. Examples of Poincaré maps for this case are given in Fig. 5.

The second case takes place when the energies are close to zero and when the parameters $\bar{\Omega}^2$ and b lie in the region of gyroscopic stabilization of equilibrium points, which are hatched in Fig. 3. In this case, Hill's regions are unbounded (see Fig. 4). However, in phase space there exists a region of bounded motion. This region forms near a stable periodic solution arising from the stable equilibrium point $x_1 = x_2 = 0$. Examples of the corresponding Poincaré maps are given in Fig. 6.

Using a Poincaré section, we first show that in the general case (when $\Omega \neq 0$) the system (2.3) without friction is nonintegrable both when $b > 0$ and when $b < 0$. For this purpose, in Fig. 7 we have constructed separatrices to unstable periodic solutions. Their transverse intersection serves as a numerical proof of the nonintegrability of the system.

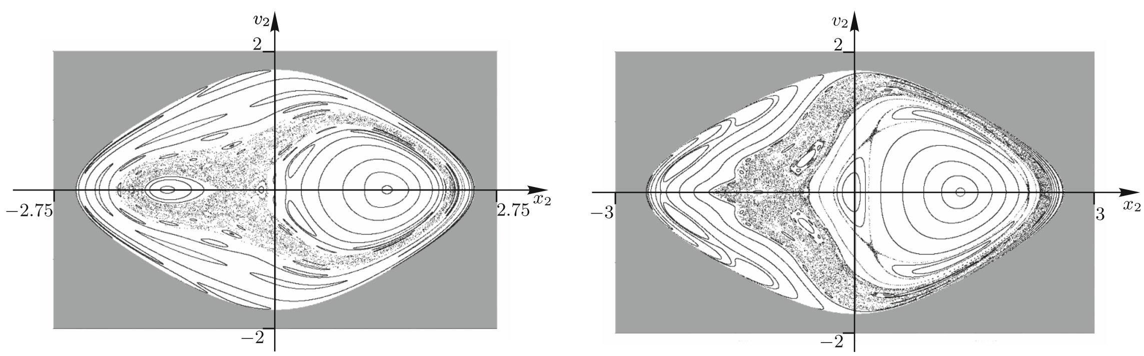

(a) $\overline{\Omega} = 0.1$, $h = 1.5$ (b) $\overline{\Omega} = 0.25$, $h = 1.5$

Fig. 5. A Poincaré map of the system (2.2), (2.3) for $b = 0.5$ and different values of Ω, h.

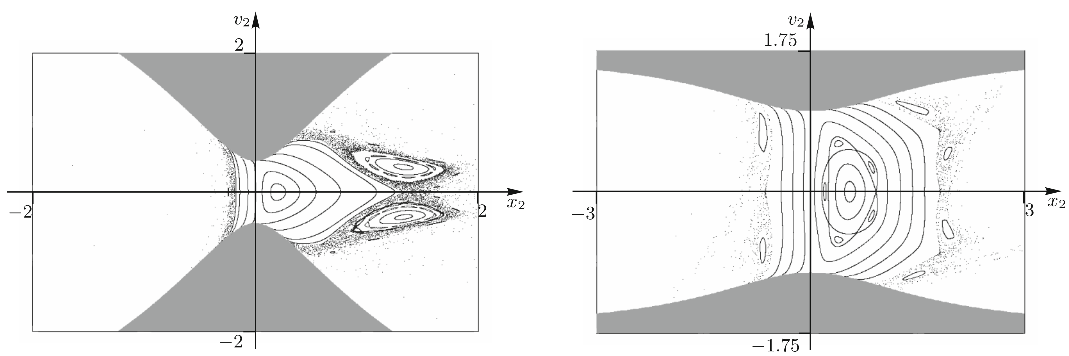

(a) $\overline{\Omega} = 2$, $h = 0.1$ (b) $\overline{\Omega} = 1.1$, $h = 0.5$

Fig. 6. A Poincaré map of the system (2.2), (2.3) for $b = 0.5$ and different values of Ω, h.

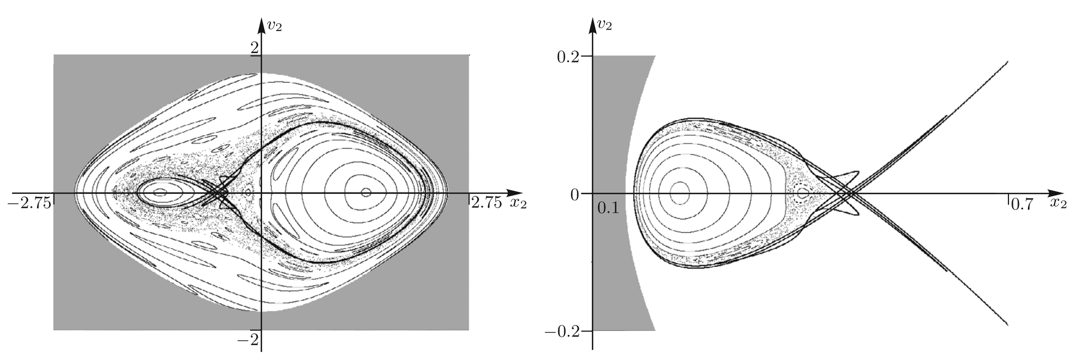

(a) $b > 0$ (b) $b < 0$

Fig. 7. A Poincaré map of the system (2.2), (2.3) for a) $b = 0.5$, $\Omega = 0.1$, $h = 1.5$; b) $b = -0.5$, $\Omega = 1.5$, $h = -0.03$. Grey denotes the regions of impossibility of motion, and the heavy lines indicate separatrices.

It can be seen from Figs. 6 and 7 that, when $b < 0$, a region of bounded trajectories can arise in a neighborhood of the saddle point of the hyperbolic paraboloid. We examine it in detail at two fixed values of the parameter b:

– $b = -0.5$, see Figs. 8 and 10a;

– $b = -1.5$, see Figs. 9 and 10b.

The numerical analysis has yielded the following results:

– in some range of values of Ω, h (see Figs. 8, 9) in a neighborhood of the saddle point of the hyperbolic paraboloid there exists an unstable periodic solution γ_0'';

– one pair of separatrices to these solutions γ_0'' bounds the region of trajectories which remain at all times in a neighborhood of the saddle point of the paraboloid.

The regions of existence of solutions γ_0'' and hence of regions of motion on the plane (Ω, h) are shown in Fig. 10a, 10b for the values $b = -0.5$ and $b = -1.5$, respectively.

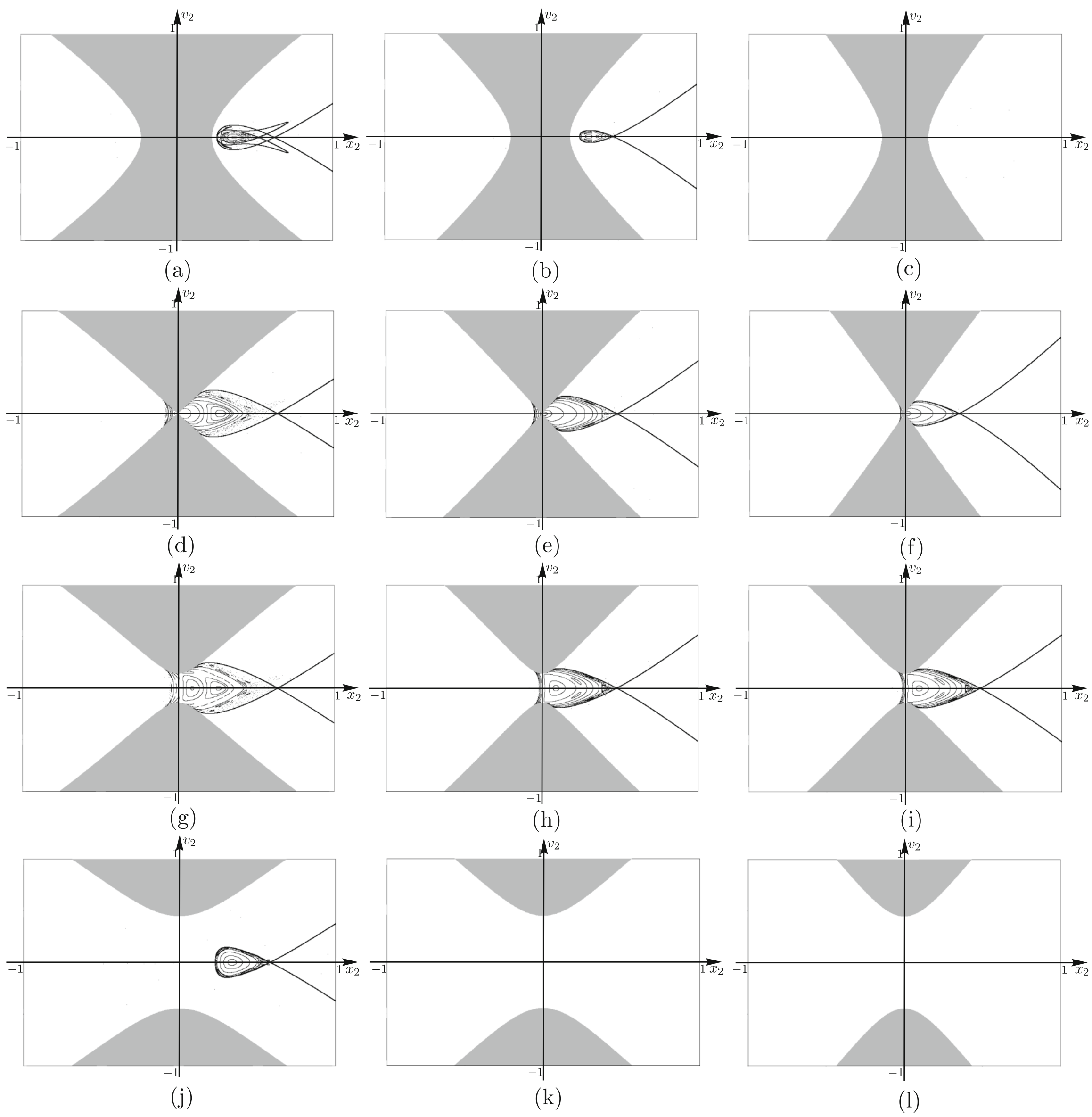

Fig. 8. A Poincaré map of the system (2.2), (2.3) for $b = -0.5$ and a) $h = -0.05$, $\Omega = 1.2$; b) $h = -0.05$, $\Omega = 1.5$; c) $h = -0.05$, $\Omega = 2$; d) $h = 0$, $\Omega = 1.2$; e) $h = 0$, $\Omega = 1.5$; f) $h = 0$, $\Omega = 2$; g) $h = 0.01$, $\Omega = 1.2$; h) $h = 0.01$, $\Omega = 1.5$; i) $h = 0.01$, $\Omega = 2$; j) $h = 0.1$, $\Omega = 1.2$; k) $h = 0.1$, $\Omega = 1.5$; l) $h = 0.1$, $\Omega = 2$. Grey denotes the regions of impossibility of motion, and the heavy lines indicate the separatrices that bound the regions of bounded motion.

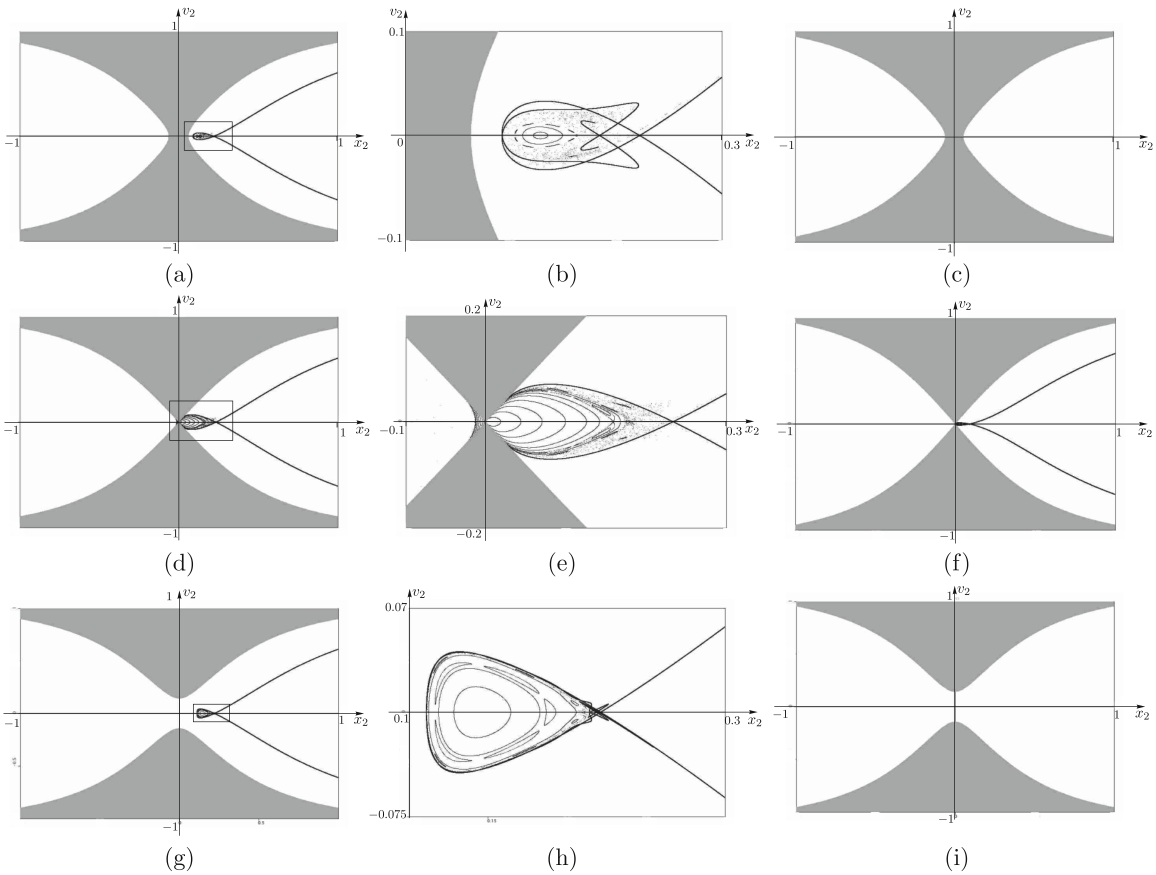

Fig. 9. A Poincaré map of the system (2.2), (2.3) and their enlarged fragments (Fig. b), e), h)) for $b = -1.5$ and a), b) $h = -0.005$, $\Omega = 1.05$; c) $h = -0.005$, $\Omega = 1.2$; d), e) $h = 0$, $\Omega = 1.05$; f) $h = 0$, $\Omega = 1.2$; g), h) $h = 0.01$, $\Omega = 1.05$; i) $h = 0.01$, $\Omega = 1.2$. Grey denotes the regions of impossibility of motion, and the heavy lines indicate the separatrices that bound the regions of bounded motion.

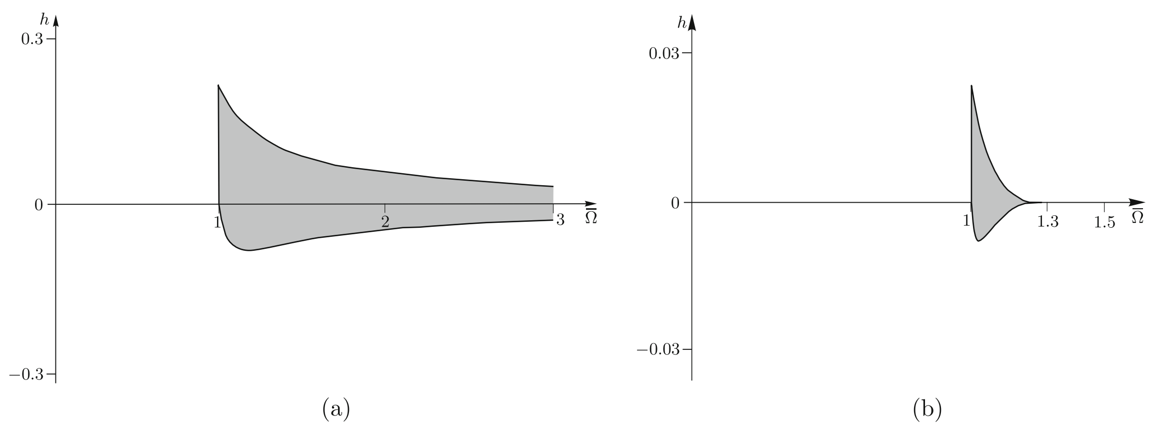

Fig. 10. Numerically plotted regions of existence of bounded motion (grey) on the plane (Ω, h) for a) $b = -0.5$; b) $b = -1.5$.

4. MOTION OF A PARTICLE WITH FRICTION

As noted in Section 2.1, the previous paper [16] dealt with the forces of internal and external viscous friction. We consider the case where these forces act simultaneously:

$$\boldsymbol{Q}^{(0)} = -\mu_1 \dot{\boldsymbol{r}} - \mu_2(\dot{\boldsymbol{r}} + \Omega \boldsymbol{e}_3 \times \boldsymbol{r}) = -\mu(\dot{\boldsymbol{r}} + \delta\Omega \boldsymbol{e}_3 \times \boldsymbol{r}),$$

$$\mu = \mu_1 + \mu_2, \quad \delta = \frac{\mu_2}{\mu_1 + \mu_2},$$

where $\boldsymbol{Q}^{(0)} = \left(Q_1^{(0)}, Q_2^{(0)}, Q_3^{(0)}\right)$, $\boldsymbol{r} = (x_1, x_2, x_3)$, $\boldsymbol{e}_3 = (0, 0, 1)$ are three-dimensional vectors. The parameter μ characterizes the general coefficient of friction, and δ characterizes the contribution of external friction (for example, air drag) to the general friction.

4.1. Stability of the Equilibrium Point

Projecting the system onto the area $\mathbb{R}^2 = \{\boldsymbol{x} = (x_1, x_2)\}$ and linearizing it in a neighborhood of the origin of coordinates, we obtain the linearized system (2.7), which in this case has the form

$$\dot{\boldsymbol{x}} = \boldsymbol{v}, \quad \dot{\boldsymbol{v}} = -\hat{\mathbf{C}}\boldsymbol{x} + \hat{\mathbf{D}}\boldsymbol{x} - \hat{\boldsymbol{\mu}}\boldsymbol{v} + \hat{\boldsymbol{\omega}}\boldsymbol{v},$$

$$\hat{\mathbf{C}} = \begin{pmatrix} g - \Omega^2 & 0 \\ 0 & gb - \Omega^2 \end{pmatrix}, \quad \hat{\mathbf{D}} = \begin{pmatrix} 0 & \mu\delta\Omega \\ -\mu\delta\Omega & 0 \end{pmatrix}, \quad \hat{\boldsymbol{\mu}} = \begin{pmatrix} \mu & 0 \\ 0 & \mu \end{pmatrix}, \quad \hat{\boldsymbol{\omega}} = \begin{pmatrix} 0 & 2\Omega \\ -2\Omega & 0 \end{pmatrix}.$$

Calculating the characteristic polynomial of this system, $P(\lambda)$, and the minor Δ_3 of the Hurwitz matrix (see the Appendix)

$$P(\lambda) = \lambda^4 + a_1\lambda^3 + a_2\lambda^2 + a_3\lambda + a_4, \quad \Delta_3 = a_1a_2a_3 - a_1^2a_4 - a_3^2,$$

we obtain stability conditions in the form

$$\begin{gathered} a_1 = 2\mu > 0, \quad a_2 = 2\Omega^2 + g(1+b) + \mu^2 > 0, \quad a_3 = \mu\big(2(2\delta - 1)\Omega^2 + g(1+b)\big) > 0, \\ a_4 = (g - \Omega^2)(bg - \Omega^2) + \mu^2\delta^2\Omega^2 > 0, \\ \Delta_3 = \mu^2\Big(2\big(2(1-\delta)^2\Omega^2 + g(1+b)\big)(4\Omega^2 + \mu^2) + g^2(1-b)^2\Big) > 0. \end{gathered} \tag{4.1}$$

By analogy with the dimensionless angular velocity $\bar{\Omega}$, we determine the dimensionless coefficient of friction

$$\bar{\mu} = \frac{\mu}{\sqrt{g}}.$$

When $\delta = 0$ and $\delta = 1$, relations (4.1) simplify considerably and we obtain the stability conditions presented in [16], see Table 1.

Table 1. Conditions for stability of the equilibrium point in the case of internal ($\delta = 0$) or external friction ($\delta = 1$).

$\delta = 0$	$\delta = 1$
$0 < b$, $\bar{\Omega}^2 < \min(1, b)$	$\bar{\Omega}^2 > -\frac{1}{2}(1+b)$, $\bar{\Omega}^2 + \frac{1}{4}\bar{\mu}^2 < -\frac{(1-b)^2}{8(1+b)}$ for $b < -1$, $b > \bar{\Omega}^2 + \bar{\mu}^2 + \frac{\bar{\mu}^2}{\bar{\Omega}^2 - 1}$ for $\bar{\Omega}^2 < 1$, $b < \bar{\Omega}^2 + \bar{\mu}^2 + \frac{\bar{\mu}^2}{\bar{\Omega}^2 - 1}$ for $1 < \bar{\Omega}^2$.

We first discuss briefly the main features typical of purely internal ($\delta = 0$) and purely external friction ($\delta = 1$), and then we point out the main characteristics of the general case (4.1).

As can be seen from Table 1, when $\delta = 0$, the stability region on the plane $(\bar{\Omega}^2, b)$ coincides with the stability region without friction in which no gyroscopic stabilization arose (see Fig. 3, grey unhatched region). This is consistent with the well-known Thomson–Tait theorem [56, p. 391]. Thus, when internal friction is added, the stability regions deform abruptly, i.e., as the friction coefficient tends to zero, none of the solutions in the region of gyroscopic stabilization can become stable.

When $\delta = 1$, the situation is quite different. As can be seen from Fig. 11, the region of stability of the Hamiltonian system ($\mu = 0$, see Fig. 3) deforms *continuously* as μ increases.

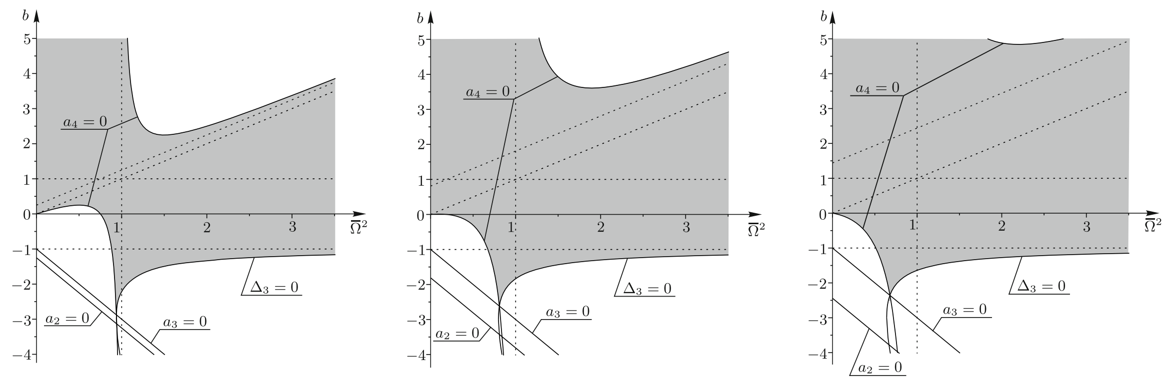

(a) $\overline{\mu} = 0.5$ (b) $\overline{\mu} = 0.9$ (c) $\overline{\mu} = 1.2$

Fig. 11. Evolution of the stability regions of the equilibrium point only with external damping ($\delta = 1$) when the damping coefficient increases.

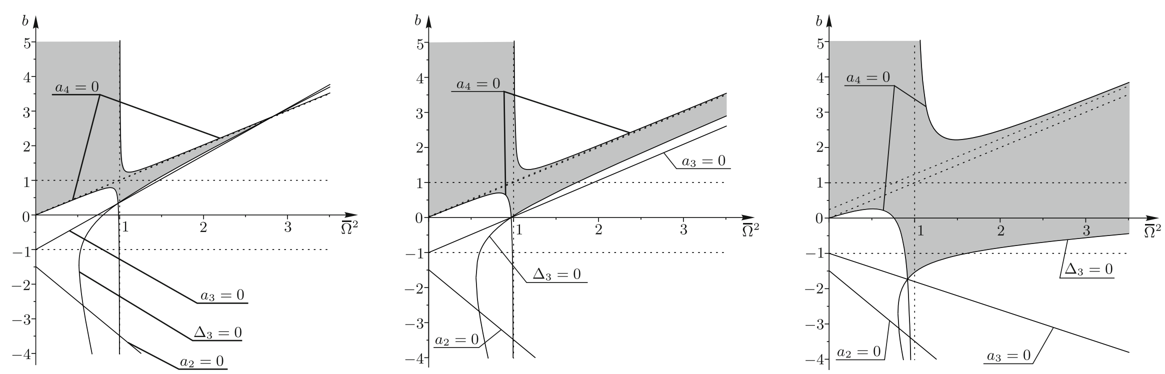

(a) $\delta = 0.16$ (b) $\delta = \delta_c \approx 0.243$ (c) $\delta = 0.7$

Fig. 12. Evolution of the stability regions of the equilibrium point for the fixed coefficient of total friction ($\mu = 0.7$) and for the changing contribution of external damping.

4.2. Numerical Analysis

For numerical investigation of the dynamics of the system with friction we use the method of constructing a three-dimensional Poincaré map. We choose the plane $x_1 = 0$ as a secant, just as we did when we constructed two-dimensional maps. We will construct the map in the space of the remaining variables (x_2, v_2, v_1).

Figure 13 shows examples of several trajectories on a three-dimensional Poincaré map. The initial conditions for these trajectories have been chosen in the region of bounded motion for the problem without friction with the same parameters (Fig. 8e).

The results of numerical experiments show that, in the case of purely internal friction, all trajectories near the fixed point $x_1 = x_2 = 0$ go to infinity ($\delta = 0$).

If the initial conditions are chosen in the region of bounded motion for the frictionless problem, then the motion can be divided into two stages. At the first stage, the trajectory approaches the stable invariant manifold (separatrix) of the fixed point. The trajectory can pass fairly close to the fixed point, and the time of approach can be fairly large at small coefficients of friction. At the second stage, the trajectory of motion along the separatrix goes to infinity. At small coefficients of friction such behavior can be regarded as temporal stability of the fixed point. This raises the question of the time of stability during which the point remains near the top of the saddle.

In the case of purely external friction ($\delta = 1$), two situations are possible depending on the stability of the fixed point $x_1 = x_2 = 0$. In the case of an unstable fixed point (uncolored regions in Fig. 11), all trajectories of motion near this point go almost right away to infinity.

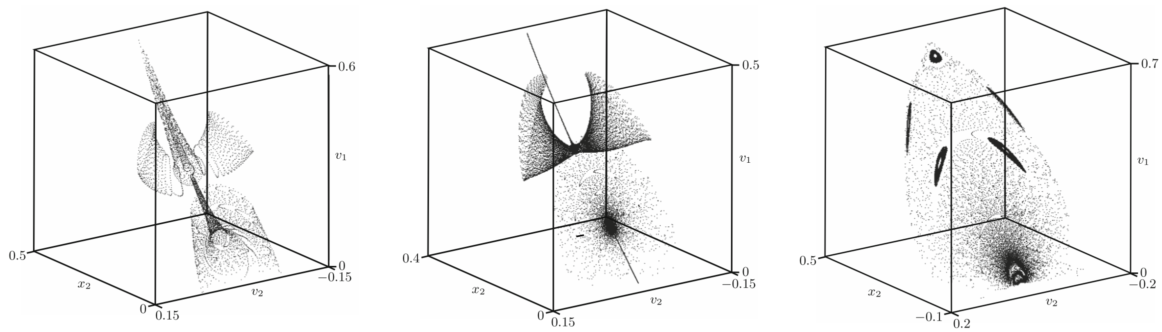

(a) $\delta = 0$ (b) $\delta = 0.65$ (c) $\delta = 1$

Fig. 13. Examples of trajectories on a three-dimensional Poincaré map for $b = -0.5$, $\Omega = 1.5$, $\mu = 0.0001$ and different values of δ.

In the case of a stable fixed point (grey regions in Fig. 11), a region of bounded motion (attraction) arises near it. It is interesting that in this case not only the fixed point itself is asymptotically stable, but attracting periodic solutions (limit cycles) of different orders also arise near this point. Such a situation is shown in Fig. 13c. In this figure, one can see two attracting limit cycles of first order and one of third order.

In the case of mixed friction, as the contribution of external friction increases, one can observe a transition from the effect of temporal stability of the fixed point to the formation of a region of bounded motion (attraction) near this point. At some values of δ these two types of behavior can coexist. Figure 13b gives an example of a Poincaré map in which one can simultaneously observe both the region of bounded motion (attraction) near the fixed point and the effect of temporal stability. A more detailed analysis of this problem can be carried out, for example, by plotting charts of dynamical regimes [28, 41, 54].

APPENDIX. LINEAR NEWTONIAN SYSTEMS — THE PROPERTY OF BEING HAMILTONIAN AND STABILITY

Let us consider systems which describe the motion of a material point on the plane $\mathbb{R}^2 = \big\{\boldsymbol{x} = (x_1, x_2)\big\}$ under the action of given forces:

$$\ddot{\boldsymbol{x}} = \boldsymbol{F}(\boldsymbol{x}, \dot{\boldsymbol{x}}).$$

Suppose that the forces are linear in $\boldsymbol{x}$ and $\dot{\boldsymbol{x}}$.

Denoting $\dot{\boldsymbol{x}} = (v_1, v_2)$, we represent this system in matrix form

$$\dot{\boldsymbol{z}} = \mathbf{A}\boldsymbol{z}, \quad \mathbf{A} = \left(\begin{array}{c|c} 0 & \mathbf{E} \\ \hline -\hat{\mathbf{C}} + \hat{\mathbf{D}} & -\hat{\boldsymbol{\mu}} + \hat{\boldsymbol{\omega}} \end{array}\right), \tag{A.1}$$

where $\boldsymbol{z} = (x_1, x_2, v_1, v_2)$ and $\mathbf{E}$ is the 2×2 identity matrix. Assume that

$$\hat{\mathbf{C}} = \begin{pmatrix} c_1 & 0 \\ 0 & c_2 \end{pmatrix}, \ \hat{\mathbf{D}} = \begin{pmatrix} 0 & -d \\ d & 0 \end{pmatrix}, \ \hat{\boldsymbol{\mu}} = \begin{pmatrix} \mu_{11} & \mu_{12} \\ \mu_{12} & \mu_{22} \end{pmatrix}, \ \hat{\boldsymbol{\omega}} = \begin{pmatrix} 0 & -\omega \\ \omega & 0 \end{pmatrix}. \tag{A.2}$$

The diagonalization of the matrix $\hat{\mathbf{C}}$ is achieved by a suitable rotation of the plane (x_1, x_2).

The physical meaning is this:

– the matrix $\hat{\mathbf{C}}$ corresponds to potential forces with the potential energy $U = \frac{1}{2}(\boldsymbol{x}, \hat{\mathbf{C}}\boldsymbol{x})$;
– the matrix $\hat{\mathbf{D}}$ defines the so-called circulatory forces [37];
– the matrix $\hat{\boldsymbol{\mu}}$ describes dissipation;
– the matrix $\hat{\boldsymbol{\omega}}$ describes gyroscopic forces.

The characteristic polynomial of the system (A.1) can be written in terms of the coefficients of the matrices as follows:

$$P = \lambda^4 + a_1\lambda^3 + a_2\lambda^2 + a_3\lambda + a_4$$
$$a_1 = \mathrm{Tr}\hat{\boldsymbol{\mu}}, \quad a_2 = c_1 + c_2 + \omega^2 + \det\hat{\boldsymbol{\mu}}, \quad a_3 = 2d\omega + c_1\mu_{22} + c_2\mu_{11}, \tag{A.3}$$
$$a_4 = c_1c_2 + d^2.$$

1. Explicit Hamiltonian Representation

We start the analysis of the system (A.1) from a particular case where the characteristic polynomial is even: $P(\lambda) = P(-\lambda)$. Obviously, it is biquadratic:

$$P(\lambda) = \lambda^4 + a_2\lambda^2 + a_4.$$

According to (A.3), in this case the parameters of the matrices (A.1) satisfy the relations

$$\mu_{11} = -\mu_{22}, \quad 2d\omega = \mu_{11}(c_1 - c_2). \tag{A.4}$$

On the one hand, it is well known that the evenness property is possessed by the characteristic polynomial for Hamiltonian systems. On the other hand, we see that, in the general case, conditions (A.4) do not guarantee that the force $\boldsymbol{F}(\boldsymbol{x}, \dot{\boldsymbol{x}})$ is purely potential (if $d \neq 0$) and purely gyroscopic (if $\hat{\boldsymbol{\mu}} \neq 0$). For this reason, such a system is sometimes regarded as nonconservative.

However, it turns out that in this case the system is Hamiltonian, more precisely, bi-Hamiltonian [1]. To show this, we will search for a representation of the system in the following (generalized) Hamiltonian form:

$$\dot{\boldsymbol{z}} = \mathbf{J}\frac{\partial H}{\partial \boldsymbol{z}},$$

where $\mathbf{J}$ is a constant nondegenerate skew-symmetric 4×4 matrix and $H(\boldsymbol{z})$ is a homogeneous quadratic function that is nondegenerate in $\boldsymbol{z}$. As is well known [1], such a system can also be written in canonical form. However, it can turn out that the canonical variables are given in terms of the initial $\boldsymbol{z}$ in a fairly complicated way, and so we do not discuss this question here. An analysis of the problems of the existence and independence of first integrals in multidimensional linear Hamiltonian systems that have not been represented in canonical form is carried out in [40].

We first show that in this case the system possesses an integral of motion that is necessary for the Hamiltonian representation.

Proposition. *The system* (A.1) *admits under conditions* (A.4) *a two-parameter family of first integrals*

$$H = \alpha_1 H_1 + \alpha_2 H_2,$$

where α_1 and α_2 are arbitrary constants, and H_1 and H_2 are independent quadratic integrals of motion

$$\begin{aligned} H_1 = {}& \frac{1}{2}(\omega - \mu_{12})\big(v_1^2 + c_1x_1^2\big) + \frac{1}{2}(\omega + \mu_{12})\big(v_2^2 + c_2x_2^2\big) + \mu_{11}v_1v_2 \\ & -\frac{1}{2}d\mu_{11}x_1^2 + \frac{1}{2}d\mu_{11}x_2^2 - \frac{1}{2}(2d\mu_{12} - c_1\mu_{11} - c_2\mu_{11})x_2x_1, \\ H_2 = {}& \frac{1}{2}(c_1 - c_2)\big(v_1^2 + c_1x_1^2\big) + dv_1v_2 + (\omega + \mu_{12})(dv_1x_1 + dv_2x_2 + c_1v_2x_1 - c_2v_1x_2) \\ & -\frac{1}{2}\Big(c_1(\omega^2 - \mu_{12}^2) + d\big(d - (\omega + \mu_{12})\mu_{11}\big)\Big)x_1^2 - \frac{1}{2}\Big(c_2(\omega + \mu_{12})^2 \\ & -d\big(d - (\omega + \mu_{12})\mu_{11}\big)\Big)x_2^2 + \left(d\mu_{12}^2 - \frac{1}{2}\omega\mu_{11}(c_1 + c_2) - c_2\mu_{11}\mu_{12} + dc_1\right)x_1x_2. \end{aligned} \tag{A.5}$$

The proof is by straightforward verification.

We now turn our attention to constructing the matrix $\mathbf{J}$. Using the integrals (A.5), we choose the parameters α_1 and α_2 in such a way that the matrix $\mathbf{J}$ looks the simplest. There are three different cases:

1. $d \neq 0,\ \omega = \dfrac{\mu_{11}}{2d}(c_1 - c_2);$

2. $d = 0,\ \mu_{11} = 0;$

3. $d = 0,\ c_1 = c_2.$

Here are examples of the simplest symplectic structures and Hamiltonians for each of the cases.

1. $d \neq 0.$

$$\mathbf{J} = \alpha^{-1}\begin{pmatrix} 0 & -2\mu_{11} & 2d & 0 \\ 2\mu_{11} & 0 & 0 & -2d \\ -2d & 0 & 0 & 2d\mu_{12} - (c_1 + c_2)\mu_{11} \\ 0 & 2d & (c_1 + c_2)\mu_{11} - 2d\mu_{12} & 0 \end{pmatrix},$$
$$\alpha = \left(-2d\mu_{11}\mu_{12} + c_1\mu_{11}^2 + c_2\mu_{11}^2 + 2d^2\right) \tag{A.6}$$
$$H = \left(d + (\omega - \mu_{12})\mu_{11}\right)v_1^2 - \left(d - (\omega + \mu_{12})\mu_{11}\right)v_2^2 + 2\mu_{11}^2 v_1 v_2$$
$$+2\mu_{11}(dv_1x_1 + dv_2x_2 + c_1v_2x_1 - c_2v_1x_2) + 2d^2x_1x_2 + dc_1x_1^2 - dc_2x_2^2,$$

where we also assume that $\alpha \neq 0$.

2. $d = 0,\ \mu_{11} = 0.$

$$\mathbf{J} = \begin{pmatrix} 0 & 0 & \frac{1}{\omega - \mu_{12}} & 0 \\ 0 & 0 & 0 & \frac{1}{\omega + \mu_{12}} \\ -\frac{1}{\omega - \mu_{12}} & 0 & 0 & -1 \\ 0 & -\frac{1}{\omega + \mu_{12}} & 1 & 0 \end{pmatrix}, \tag{A.7}$$
$$H = (\omega - \mu_{12})\left(v_1^2 + c_1x_1^2\right) + (\omega + \mu_{12})(c_2x_2^2 + v_2^2),$$

where we assume $\omega \neq \mu_{12}$ and $\omega \neq -\mu_{12}$.

3. $d = 0,\ c_1 = c_2.$

$$\mathbf{J} = \begin{pmatrix} 0 & -\frac{1}{c_1} & 0 & 0 \\ \frac{1}{c_1} & 0 & 0 & 0 \\ 0 & 0 & 0 & -1 \\ 0 & 0 & 1 & 0 \end{pmatrix}, \tag{A.8}$$
$$H = (\omega - \mu_{12})v_1^2 + (\omega + \mu_{12})v_2^2 + 2\mu_{11}v_1v_2 - 2v_1c_1x_2 + 2v_2c_1x_1,$$

where we assume $c_1 \neq 0$.

Remark. This implies that in the linear approximation all systems of Newtonian type

$$\ddot{\boldsymbol{x}} = \boldsymbol{F}(\boldsymbol{x}), \quad \boldsymbol{x} = (x_1, x_2), \quad \boldsymbol{F}(0) = 0$$

turn out to be conservative even if $\operatorname{rot}\boldsymbol{F} = \left(\dfrac{\partial F_1}{\partial x_2} - \dfrac{\partial F_2}{\partial x_1}\right)\Big|_{\boldsymbol{x}=0} = d \neq 0.$

The roots of the characteristic polynomial (A.3) are complex conjugate and symmetric relative to the complex axis. Their arrangement on the complex plane and the corresponding type of the fixed point of the system (A.1) are shown in Fig. 14 as functions of the coefficients (a_2, a_4). Consequently,

in the case (A.4) *the stability conditions are written in terms of the coefficients of the matrices* (A.2) *in the form*

$$c_1c_2 + d^2 > 0, \quad (c_1 + c_2 + \omega^2 - \mu_{11}^2 - \mu_{12}^2)^2 - 4(c_1c_2 + d^2) > 0,$$
$$c_1 + c_2 + \omega^2 - \mu_{11}^2 - \mu_{12}^2 > 0.$$

We note that the first two inequalities $(a_4 > 0,\ a_2^2 - 4a_4 > 0)$ define in the parameter space the set $\mathcal{S}^{(0)}$, which is, as a rule, disconnected and consists of several (disjoint) connectedness components

$$\mathcal{S}^{(0)} = S_1 \cup S_2 \cup \ldots \cup S_l.$$

The last inequality $(a_2 > 0)$ allows one to single out among these connectedness components those in which stability is observed.

Remark. Since the flow of the system in this case preserves the phase volume $(\mathrm{Tr}\hat{\boldsymbol{\mu}} = 0)$, the equilibrium point cannot be asymptotically stable.

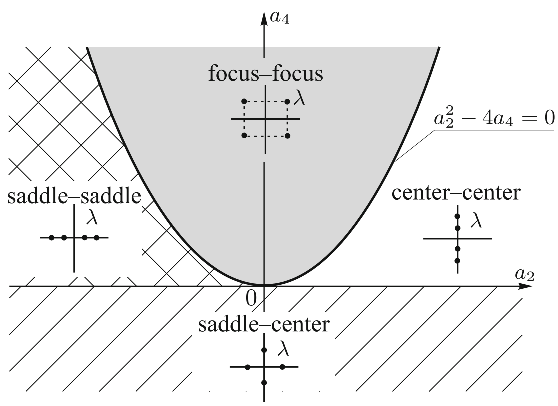

Fig. 14

2. The Case $\hat{\mathbf{D}} = 0$ *and the Case of Complete Dissipation. Thomson – Tait Theorems*

We assume that $\hat{\mathbf{D}} = 0$ (there are no circulatory forces), and the dissipation matrix $\hat{\boldsymbol{\mu}}$ is nondegenerate and positive definite. We also assume that the matrix $\hat{\mathbf{C}}$ is nondegenerate since otherwise the equilibrium point is degenerate and its stability requires a separate analysis.

The conditions for stability of the equilibrium point can be represented in the form of Table 2, which expresses the content of the well-known Thomson – Tait [56] (Kelvin) theorems for this situation.

3. The General Case

In the general case, the stability analysis of an equilibrium point is usually carried out using a pair of the most widespread criteria, which we present here for the system (A.1).

The Routh – Hurwitz criterion. To use it, we need to obtain the minors of the Hurwitz matrix from the coefficients of the characteristic polynomial (A.3)

$$\boldsymbol{\Gamma} = \begin{Vmatrix} a_1 & 1 & 0 & 0 \\ a_3 & a_2 & a_1 & 1 \\ 0 & a_4 & a_3 & a_2 \\ 0 & 0 & 0 & a_4 \end{Vmatrix}.$$

Table 2. Thomson – Tait [56] (Kelvin) stability conditions, as applied to the system (A.1).

	Existence of additional terms		Stability conditions (additional remarks)
	$\hat{\boldsymbol{\omega}}$	$\hat{\boldsymbol{\mu}}$	
1	−	−	$c_1 > 0$, $c_2 > 0$
2	+	−	1. $c_1 > 0$, $c_2 > 0$ 2. $c_1 < 0$, $c_2 < 0$, $\omega^2 > \left(\sqrt{\lvert c_1\rvert} + \sqrt{\lvert c_2\rvert}\right)^2$
3	−	+	$c_1 > 0$, $c_2 > 0$ (the equilibrium point is asymptotically stable)
4	+	+	$c_1 > 0$, $c_2 > 0$ (the equilibrium point is asymptotically stable)

For all roots of the characteristic polynomial (A.3) with real coefficients to have a negative real part, it is necessary and sufficient that all princial minors $\Delta_2, \ldots, \Delta_4$ of the matrix $\mathbf{\Gamma}$ be positive.

Noting that $\Delta_4 = a_4 \cdot \Delta_3$, we obtain four inequalities in explicit form

$$\begin{gathered} a_1 > 0, \quad a_4 > 0, \quad \Delta_2 = a_1 a_2 - a_3 > 0, \\ \Delta_3 = a_1 a_2 a_3 - a_1^2 a_4 - a_3^2 > 0. \end{gathered} \tag{A.9}$$

The Lienard – Shepherd criterion. Combining inequalities (A.9), one can obtain a different set of inequalities

$$\begin{gathered} a_k > 0,\ k = 1, \ldots, 4, \\ \Delta_3 = a_1 a_2 a_3 - a_1^2 a_4 - a_3^2 > 0. \end{gathered} \tag{A.10}$$

General scheme of stability analysis. It should be kept in mind that not all of these inequalities play the same role in defining the stability region. In the parameter space $\boldsymbol{\alpha} = (\alpha_1, \ldots, \alpha_m)$, on which the coefficients of the characteristic polynomial $a_1(\boldsymbol{\alpha}), \ldots, a_4(\boldsymbol{\alpha})$ depend, we single out the set

$$\mathcal{S}^{(0)} = \left\{ \boldsymbol{\alpha} \mid 0 < a_4,\ 0 < a_1 a_2 a_3 - a_1^2 a_4 - a_3^2 \right\}. \tag{A.11}$$

In the general case, it is disconnected and is a union of its (intersecting) connectedness components:

$$\mathcal{S}^{(0)} = S_1 \cup S_2 \cup \ldots \cup S_l.$$

Proposition. *The stability region of the equilibrium point of the system consists of one or several connectedness components of the set* $\mathcal{S}^{(0)}$.

Proof. Consider two sets in the parameter space which are given by the relations

$$\begin{gathered} \mathcal{D}_+ = \{ \boldsymbol{\alpha} \,|\, 0 < a_1(\boldsymbol{\alpha}), 0 < a_2(\boldsymbol{\alpha}), 0 < a_3(\boldsymbol{\alpha}) \}, \\ \mathcal{D}^{(0)} = \{ \boldsymbol{\alpha} \,|\, a_1(\boldsymbol{\alpha}) = 0 \} \cup \{ \boldsymbol{\alpha} \,|\, a_2(\boldsymbol{\alpha}) = 0 \} \cup \{ \boldsymbol{\alpha} \,|\, a_3(\boldsymbol{\alpha}) = 0 \}. \end{gathered}$$

According to (A.11), an arbitrary point $\boldsymbol{\alpha} \in \mathcal{D}^{(0)}$ cannot belong to the set $\mathcal{S}^{(0)}$. Hence, if $\mathcal{S}_k$ is the connectedness component $\mathcal{S}^{(0)}$, then it either entirely belongs to $\mathcal{D}_+$ or entirely lies outside $\mathcal{D}_+$. $\square$

Thus, the algorithm of stability analysis of the equilibrium point reduces to constructing the set $\mathcal{S}^{(0)}$ *given by the pairs of inequalities*

$$0 < a_4, \quad 0 < a_1 a_2 a_3 - a_1^2 a_4 - a_3^2$$

and by a subsequent elimination of those of its connectedness components which do not satisfy the inequalities

$$0 < a_1, \quad 0 < a_2, \quad 0 < a_3.$$

Remark. Instead of the three inequalities $0 < a_k, \quad k = 1, 2, 3$, one can use a pair of inequalities from the Routh – Hurwitz criterion

$$0 < a_1, \quad 0 < \Delta_2 < a_1 a_2.$$

This result can also be obtained as a consequence of the general statement describing the boundaries of the stability region, which is ascribed to Hurwitz:

the boundary of the stability region of an equilibrium point is given by the relations

$$\Delta_n = a_n \Delta_{n-1} = 0,$$
$$0 < \Delta_1, \ldots, 0 < \Delta_{n-2}.$$

Its proof is based on Orlando's formula (see [27])

$$\Delta_n = (-1)^{\frac{n(n+1)}{2}} \lambda_1 \lambda_2 \ldots \lambda_n \prod_{i<k}^{n} (\lambda_i + \lambda_k),$$

where λ_i are the roots of the characteristic polynomial.

ACKNOWLEDGMENTS

The authors express their gratitude to V. V. Kozlov and I. A. Bizyaev for fruitful discussions and useful comments.

FUNDING

The work of A. V. Borisov is supported by the program of the Presidium of the Russian Academy of Sciences no. 01 "Fundamental Mathematics and its Applications". The work of A. A. Kilin (Section 3.2 and Appendix 1) is supported by the RSF grant no. 15-12-00235. The work of I. S. Mamaev is carried out at MIPT under project 5–100 for state support for leading universities of the Russian Federation.

CONFLICT OF INTEREST

The authors declare that they have no conflicts of interest.

REFERENCES

1. Arnol'd, V. I., Kozlov, V. V., and Neĭshtadt, A. I., *Mathematical Aspects of Classical and Celestial Mechanics,* 3rd ed., Encyclopaedia Math. Sci., vol. 3, Berlin: Springer, 2006.
2. Bizyaev, I. A., Borisov, A. V., Kozlov, V. V, and Mamaev, I. S., Fermi-Like Acceleration and Power-Law Energy Growth in Nonholonomic Systems, *Nonlinearity,* 2019, in press.
3. Bloch, A. M., *Nonholonomic Mechanics and Control,* 2nd ed., Interdiscip. Appl. Math., vol. 24, New York: Springer, 2015.
4. Bloch, A. M., Krishnaprasad, P. S., Marsden, J. E., and Murray, R. M., Nonholonomic Mechanical Systems with Symmetry, *Arch. Rational Mech. Anal.,* 1996, vol. 136, no. 1, pp. 21–99.
5. Bogoyavlensky, O. I., Integrable Cases of Rigid Body Dynamics and Integrable Systems on Spheres S^n, *Izv. AN SSSR,* 1985, vol. 49, no. 5, pp. 899–915 (Russian).
6. Bolsinov, A. V., Borisov, A. V., and Mamaev, I. S., Topology and Stability of Integrable Systems, *Russian Math. Surveys,* 2010, vol. 65, no. 2, pp. 259–318; see also: *Uspekhi Mat. Nauk,* 2010, vol. 65, no. 2, pp. 71–132.
7. Borisov, A. V., Kazakov, A. O., and Kuznetsov, S. P., Nonlinear Dynamics of the Rattleback: A Nonholonomic Model, *Physics–Uspekhi,* 2014, vol. 57, no. 5, pp. 453–460; see also: *Uspekhi Fiz. Nauk,* 2014, vol. 184, no. 5, pp. 493–500.

8. Borisov, A. V., Kilin, A. A., and Mamaev, I. S., A Nonholonomic Model of the Paul Trap, *Regul. Chaotic Dyn.,* 2018, vol. 23, no. 3, pp. 339–354.
9. Borisov, A. V., Kilin, A. A., and Mamaev, I. S., Stability of Steady Rotations in the Nonholonomic Routh Problem, *Regul. Chaotic Dyn.,* 2008, vol. 13, no. 4, pp. 239–249.
10. Borisov, A. V. and Mamaev, I. S., *Modern Methods of the Theory of Integrable Systems,* Moscow: R&C Dynamics, ICS, 2003 (Russian).
11. Borisov, A. V. and Mamaev, I. S., Conservation Laws, Hierarchy of Dynamics and Explicit Integration of Nonholonomic Systems, *Regul. Chaotic Dyn.,* 2008, vol. 13, no. 5, pp. 443–490.
12. Borisov, A. V. and Mamaev, I. S., Strange Attractors in Rattleback Dynamics, *Physics–Uspekhi,* 2003, vol. 46, no. 4, pp. 393–403; see also: *Uspekhi Fiz. Nauk,* 2003, vol. 173, no. 4, pp. 407–418.
13. Borisov, A. V., Mamaev, I. S., and Bizyaev, I. A., The Hierarchy of Dynamics of a Rigid Body Rolling without Slipping and Spinning on a Plane and a Sphere, *Regul. Chaotic Dyn.,* 2013, vol. 18, no. 3, pp. 277–328.
14. Borisov, A. V., Mamaev, I. S., and Bizyaev, I. A., The Jacobi Integral in Nonholonomic Mechanics, *Regul. Chaotic Dyn.,* 2015, vol. 20, no. 3, pp. 383–400.
15. Borisov, A. V., Mamaev, I. S., and Kilin, A. A., Rolling of a Ball on a Surface: New Integrals and Hierarchy of Dynamics, *Regul. Chaotic Dyn.,* 2002, vol. 7, no. 2, pp. 201–219.
16. Bottema, O., Stability of Equilibrium of a Heavy Particle on a Rotating Surface, *Z. Angew. Math. Phys.,* 1976, vol. 27, no. 5, pp. 663–669.
17. Bou-Rabee, N. M., Marsden, J. E., Romero, L. A., Tippe Top Inversion As a Dissipation-Induced Instability, *SIAM J. Appl. Dyn. Syst.,* 2004, vol. 3, no. 3, pp. 352–377.
18. Brouwer, L. E. J., *Collected Works: Vol. 2,* H. Freudenthal (Ed.), Amsterdam: North-Holland, 1976.
19. Brouwer, L. E. J., The Motion of a Particle on the Bottom of a Rotating Vessel under the Influence of the Gravitational Force, in *Collected Works: Vol. 2,* H. Freudenthal (Ed.), Amsterdam: North-Holland, 1976, pp. 665–686.
20. Cartwright, J. H. E., Feingold, M., and Piro, O., An Introduction to Chaotic Advection, in *Mixing: Chaos and Turbulence,* H. Chaté, E. Villermaux, J.-M. Chomaz (Eds.), NATO ASI Series (Series B: Physics), vol. 373, Boston, Mass.: Springer, 1999, pp. 307–342.
21. Chaplygin, S. A., On a Paraboloid Pendulum, in *Complete Collection of Works: Vol. 1,* Leningrad: Izd. Akad. Nauk SSSR, 1933, pp. 194–199 (Russian).
22. Cheng, Ch. Q. and Sun, Y. S., Existence of Invariant Tori in Three-Dimensional Measure-Preserving Mappings, *Celestial Mech. Dynam. Astronom.,* 1989/90, vol. 47, no. 3, pp. 275–292.
23. Chetayev, N. G., *The Stability of Motion,* Oxford: Pergamon, 1961.
24. Dullin, H. R. and Meiss, J. D., Quadratic Volume-Preserving Maps: Invariant Circles and Bifurcations, *SIAM J. Appl. Dyn. Syst.,* 2009, vol. 8, no. 1, pp. 76–128.
25. Fan, W., Du, L., Wang, S., and Zhou, H., Confining Rigid Balls by Mimicking Quadrupole Ion Trapping, *Am. J. Phys.,* 2017, vol. 85, no. 11, pp. 821–829.
26. Fufaev, N. A., A Sphere Rolling on a Horizontal Rotating Plane, *J. Appl. Math. Mech.,* 1983, vol. 47, no. 1, pp. 27–29; see also: *Prikl. Mat. Mekh.,* 1983, vol. 47, no. 1, pp. 43–47.
27. Gantmacher, F. R., *The Theory of Matrices: In 2 Vols.,* New York: Chelsea, 1959.
28. Gonchenko, A. S., Gonchenko, S. V., and Kazakov, A. O., Richness of Chaotic Dynamics in Nonholonomic Models of a Celtic Stone, *Regul. Chaotic Dyn.,* 2013, vol. 18, no. 5, pp. 521–538.
29. Gray, A., Jones, A., and Rimmer, R., Motion under Gravity on a Paraboloid, *J. Differential Equations,* 1982, vol. 45, no. 2, pp. 168–181.
30. Hasegawa, T. and Bollinger, J. J., Rotating-Radio-Frequency Ion Traps, *Phys. Rev. A,* 2005, vol. 72, no. 4, 043403, 8 pp.
31. Huygens, Ch., *Horologium oscillatorium, sive De motu pendulorum ad horologia aptato demonstrationes geometricae,* Paris: Muguet, 1673.
32. Jacobi, C. G. J., *Vorlesungen über Dynamik,* 2nd ed., Berlin: Reimer, 1884.
33. Kane, T. R. and Levinson, D. A., A Realistic Solution of the Symmetric Top Problem, *ASME J. Appl. Mech.,* 1978, vol. 45, no. 4, pp. 903–909.
34. Karapetian, A. V., Global Qualitative Analysis of Tippe Top Dynamics, *Mech. Solids,* 2008, vol. 43, no. 3, pp. 342–348; see also: *Izv. Ross. Akad. Nauk. Mekh. Tverd. Tela,* 2008, no. 3, pp. 33–41.
35. Karavaev, Yu. L., Kilin, A. A., and Klekovkin, A. V., The Dynamical Model of the Rolling Friction of Spherical Bodies on a Plane without Slipping, *Nelin. Dinam.,* 2017, vol. 13, no. 4, pp. 599–609 (Russian).
36. Kirillov, O. N., Brouwer's Problem on a Heavy Particle in a Rotating Vessel: Wave Propagation, Ion Traps, and Rotor Dynamics, *Phys. Lett. A,* 2011, vol. 375, no. 15, pp. 1653–1660.
37. Kirillov, O. N., *Nonconservative Stability Problems of Modern Physics,* Berlin: de Gruyter, 2013.
38. Kirillov, O. N. and Levi, M., Rotating Saddle Trap as Foucault's Pendulum, *Am. J. Phys.,* 2016, vol. 84, no. 1, pp. 26–31.
39. Koiller, J., and Ehlers, K., Rubber Rolling over a Sphere, *Regul. Chaotic Dyn.,* 2007, vol. 12, no. 2, pp. 127–152.

40. Kozlov, V. V., Linear Hamiltonian Systems: Quadratic Integrals, Singular Subspaces and Stability, *Regul. Chaotic Dyn.,* 2018, vol. 23, no. 1, pp. 26–46.
41. Kuznetsov, A. P., Kuznetsov, S. P., Mosekilde, E., and Turukina, L. V., Two-Parameter Analysis of the Scaling Behavior at the Onset of Chaos: Tricritical and Pseudo-Tricritical Points, *Phys. A,* 2001, vol. 300, nos. 3–4, pp. 367–385.
42. Markeev, A. P., On the Theory of Motion of a Rigid Body with a Vibrating Suspension, *Dokl. Phys.,* 2009, vol. 54, no. 8, pp. 392–396; see also: *Dokl. Akad. Nauk,* 2009, vol. 427, no. 6, pp. 771–775.
43. Meiss, J. D., Miguel, N., Simó, C., and Vieiro, A., Accelerator Modes and Anomalous Diffusion in 3D Volume-Preserving Maps, arXiv:1802.10484 (2018).
44. Mireles James, J. D., Quadratic Volume-Preserving Maps: (Un)Stable Manifolds, Hyperbolic Dynamics, and Vortex-Bubble Bifurcations, *J. Nonlinear Sci.,* 2013, vol. 23, no. 4, pp. 585–615.
45. Moser, J., *Lectures on Hamiltonian systems,* vol. 81, Providence, R.I.: American Mathematical Soc., 1968.
46. Painlevé, P., *Leçons sur l'intégration des équations différentielles de la mécanique et applications,* Paris: Hermann, 1895.
47. Paul, W., Electromagnetic Traps for Charged and Neutral Particles, *Rev. Mod. Phys.,* 1990, vol. 62, no. 3, pp. 531–540.
48. Paul, W. and Steinwedel, H., Ein neues Massenspektrometer ohne Magnetfeld, *Z. Naturforsch. A,* 1953, vol. 8, no. 7, pp. 448–450.
49. Pearce, R. M., Strong Focussing in a Magnetic Helical Quadrupole Channel, *Nucl. Instrum. Methods,* 1970, vol. 83, no. 1, pp. 101–108.
50. Rauch-Wojciechowski, S., Sköldstam, M., and Glad, T., Mathematical Analysis of the Tippe Top, *Regul. Chaotic Dyn.,* 2005, vol. 10, no. 4, pp. 333–362.
51. Routh, E. J., *Dynamics of a System of Rigid Bodies: Elementary Part. Being Part 1 of a Treatise on the Whole Subject,* 7th ed., rev. and enl., New York: Dover, 1960.
52. Siegel, C. L. and Moser, J. K., *Lectures on Celestial Mechanics,* Grundlehren Math. Wiss., vol. 187, New York: Springer, 1971.
53. Sokirko, A. V., Belopolskii, A. A., Matytsyn, A. V., and Kossakowski, D. A., Behavior of a Ball on the Surface of a Rotating Disk, *Am. J. Phys.,* 1994, vol. 62, no. 2, pp. 151–156.
54. Stankevich, N. V., Kuznetsov, N. V., Leonov, G. A., and Chua, L. O., Scenario of the Birth of Hidden Attractors in the Chua Circuit, *Internat. J. Bifur. Chaos Appl. Sci. Engrg.,* 2017, vol. 27, no. 12, 1730038, 18 pp.
55. Thompson, R. I., Harmon, T. J., and Ball, M. G., The Rotating-Saddle Trap: A Mechanical Analogy to RF-Electric-Quadrupole Ion Trapping?, *Can. J. Phys.,* 2002, vol. 80, no. 12, pp. 1433–1448.
56. Thomson, W. and Tait, P. G., *A Treatise on Natural Philosophy: Vol. 1, Part 1,* Cambridge: Cambridge Univ. Press, 1879, pp. 370–415.
57. Verhulst, F., Brouwer's Rotating Vessel: 1. Stabilization, *Z. Angew. Math. Phys.,* 2012, vol. 63, no. 4, pp. 727–736.
58. Wojciechowski, S., Integrable One-Particle Potentials Related to the Neumann System and the Jacobi Problem of Geodesic Motion on an Ellipsoid, *Phys. Lett. A,* 1985, vol. 107, no. 3, pp. 106–111.
59. Yudovich, V. I., The Dynamics of a Particle on a Smooth Vibrating Surface, *J. Appl. Math. Mech.,* 1998, vol. 62, no. 6, pp. 893–900; see also: *Prikl. Mat. Mekh.,* 1998, vol. 62, no. 6, pp. 968–976.
60. https://www.youtube.com/watch?v=9TH5mFHLmfc (2016).
61. https://www.youtube.com/watch?v=pG1TcnpsY_8 (2016).